CHAPTER 8

Vehicle Nonlinear Equations of Motion

A SIX DEGREE OF FREEDOM NONLINEAR VEHICLE MODEL is developed independently of the model used for the Berkeley simulation of Section 2 and described in (Peng 1992). This effort is a continuation of the work reported in (Douglas et al. 1995). The original motivation for an independent derivation was to be sure that all assumptions, definitions and issues which underlie the Berkeley simulation model were well understood. This exercise proved worthwhile in that some differences between the model described here and the Berkeley model were uncovered. The most notable difference relates to assumptions made in the Berkeley model that make it difficult to modify to allow for changes in road slope and superelevation. These assumptions include small angle approximations, a planar road surface and that the road gradient is the same for all four wheels. These modifications are needed, for example, in the design and robustness evaluation of the health monitoring system described in Sections 3 through 7. Various other vehicle models are available, for example, in (Hedrick et al. 1993, Lukowski et al. 1990, Lukowski and Medeksza 1992, Peng 1992, Smith and Starkey 1992, Willumeit et al. 1992). But in each, some feature is missing that is important to health monitoring applications.

A common and economical approach to vehicle dynamics model development is to make simplifying assumptions and to neglect various features of the vehicle system when the loss in fidelity does not significantly affect the application of the model. For example, vehicle models developed by Smith *et al.* (Smith and Starkey 1992) use the load transfer method to model the suspension characteristics. The load transfer method models a load redistribution at the four suspension supports when the vehicle accelerates or corners. When the vehicle accelerates, the load shifts between the front and the rear suspension supports. When the vehicle corners, there is a lateral acceleration and the load shifts between the left and right suspension supports. With the load transfer approach, development of the governing equations is simplified because the suspension characteristics are not modeled directly. Model fidelity is adequate when the road is smooth and flat and when a model of the vertical motion is not important.

In the following model development, the approach is to derive the full equations of motion while making as few approximations as possible. Simplifications as allowed by specific applications are introduced later. Two features included here that are not part of the Berkeley model are a steering system and a road noise model.

This section is organized as follows. Section 8.1 contains a derivation of the vehicle longitudinal dynamics and the various subcomponents of the vehicle. In the longitudinal model, motion is restricted to longitudinal and vertical translation and pitch rotation. The applied forces and moments include those of the suspension model, the aerodynamics model, the tire traction model, the brake model, and the engine model.

Section 8.2 deals with the derivation of the full six degree of freedom vehicle model. All vehicle dynamics modes are included: longitudinal, lateral and vertical translations and roll, pitch and yaw rotations. Including kinematic relations, the system of equations is 12^{th} order. In addition, subcomponents from the longitudinal model are generalized to the full nonlinear model and a steering system and road noise model are added.

Section 8.3 presents the simulation results of the longitudinal model and the full model. In one simulation study, a comparison is made between the responses of the full nonlinear model and nonlinear model modified with small angle approximations. The study shows that small angle approximations do not contribute significant errors and are a reasonable model simplification. In another simulation study, linearized models from various operating points are obtained. Their responses are compared to those of the nonlinear model to find the size of an acceptable linear operating region. The MatLab™ computer simulation codes used in Section 8.3 are available in (Nguyen 1996).

8.1 NonLinear Longitudinal Vehicle Model

In order to gain a better understanding of vehicle dynamics and to have a simple model for simulation, a longitudinal vehicle dynamics model is developed first. In the longitudinal model, motion is restricted to longitudinal and vertical translation and pitch rotation. These dynamics couple with the engine, brake, suspension, and wheel rotational dynamics .

8.1.1 Reference Frames

Figure 8.1 shows the definition of coordinates and variables of the longitudinal model. First an Earth-fixed frame E with origin $\mathcal{O}$ is defined with unit vectors $\left(\underline{e}_x, \underline{e}_y, \underline{e}_z\right)$, where $\underline{e}_y$ points into the page. Next define the vehicle-fixed frame, having the origin C at the vehicle center of mass, with unit vectors $\left(\underline{c}_x, \underline{c}_y, \underline{c}_z\right)$ along the vehicle's principal axes. This vehicle-fixed frame is obtained by rotating the Earth-fixed frame around its axis by an angular displacement θ, the pitch angle. Finally two sets of road axes are used to describe the road surface at the front and the rear wheels. These axes are described by the unit vectors $\left(\underline{r}_{x_i}, \underline{r}_{y_i}, \underline{r}_{z_i}\right)$ with $i = 1$ and 2 referring to front and rear wheels, respectively. These road-fixed frames with unit vectors $\left(\underline{r}_{x_i}, \underline{r}_{y_i}, \underline{r}_{z_i}\right)$ are obtained by rotating the Earth-fixed frame by an amount $\Delta_i \underline{e}_y$. Hence the coordinate transformation matrices are

$$\begin{bmatrix} \underline{c}_x \\ \underline{c}_y \\ \underline{c}_z \end{bmatrix} = \begin{bmatrix} \cos\theta & 0 & -\sin\theta \\ 0 & 1 & 0 \\ \sin\theta & 0 & \cos\theta \end{bmatrix} \begin{bmatrix} \underline{e}_x \\ \underline{e}_y \\ \underline{e}_z \end{bmatrix} \tag{8.1}$$

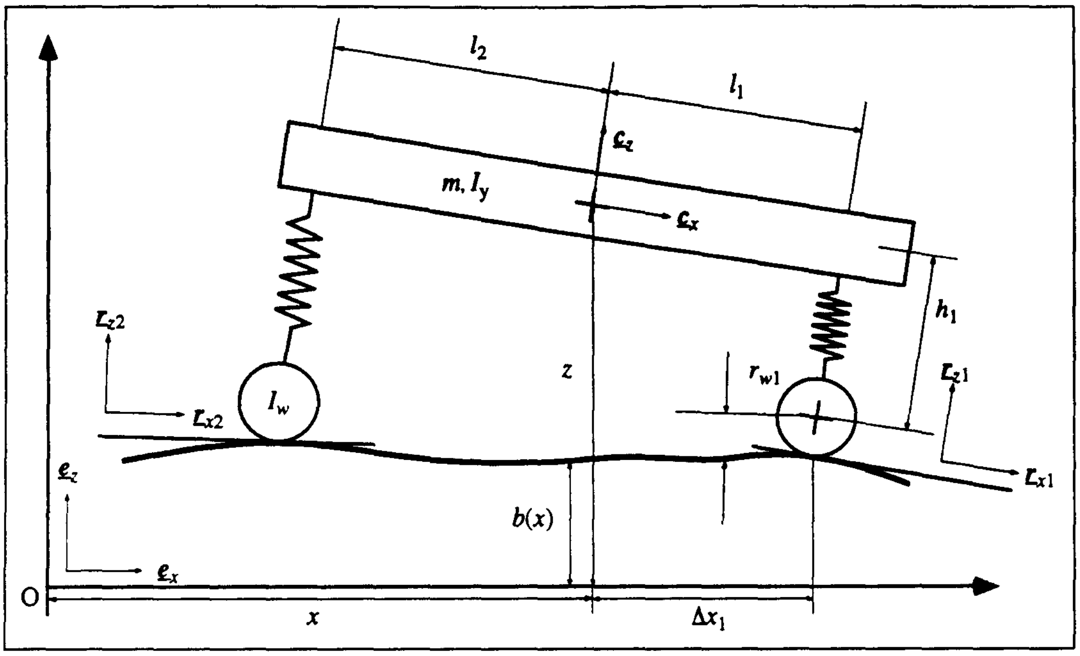

Figure 8.1: Vehicle configuration for the nonlinear longitudinal model.

$$\begin{bmatrix} \underline{r}_{x_i} \\ \underline{r}_{y_i} \\ \underline{r}_{z_i} \end{bmatrix} = \begin{bmatrix} \cos\Delta_i & 0 & -\sin\Delta_i \\ 0 & 1 & 0 \\ \sin\Delta_i & 0 & \cos\Delta_i \end{bmatrix} \begin{bmatrix} \underline{e}_x \\ \underline{e}_y \\ \underline{e}_z \end{bmatrix} \qquad i = 1, 2 \tag{8.2}$$

Note that the subscript i will be used from now on to refer to quantities that have front and rear components.

8.1.2 Vehicle Dynamics

The dynamic equations of motion are derived from Newton's law applied in an inertial reference frame. The pitch dynamics are derived first. The longitudinal and vertical translation dynamics follow.

Rotational Equations of Motion

The angular velocity of the vehicle relative to the Earth-fixed frame is given by

$$\underline{\omega} = \dot{\theta}\underline{e}_y \tag{8.3}$$

$$= \omega_y \underline{e}_y \tag{8.4}$$

The rotational kinematic equation becomes

$$\dot{\theta} = \omega_y \tag{8.5}$$

The angular acceleration follows by taking the time derivative of Equation (8.3),

$$\dot{\underline{\omega}} = \dot{\omega}_y \underline{e}_y \tag{8.6}$$

Hence the rotational dynamic equation of motion is obtained from Euler's equation,

$$\dot{\omega}_y = \frac{M_y}{I_y} \tag{8.7}$$

where M_y, which will be derived later in Section 8.1.5, is the y-axis component of the total moment applied about the vehicle center of mass by suspension and aerodynamic forces and I_y is the moment of inertia of the sprung mass around the same y-axis. The sprung mass is the portion of the vehicle that is supported by the suspension system. The remaining portion which includes the drivetrain and the wheel assemblies is known as the unsprung mass.

Translational Equations of Motion

Let $\underline{P}_{\mathrm{CM}} = x\underline{e}_x + z\underline{e}_z$ be the position vector from the Earth-fixed origin $\mathcal{O}$ to the vehicle center of mass as seen in Figure 8.1, then the velocity of the mass center can be expressed either in Earth-fixed or vehicle-fixed coordinates as

$$\underline{v}_{\mathrm{CM}} = \dot{x}\underline{e}_x + \dot{z}\underline{e}_z \tag{8.8}$$

$$= v_x \underline{c}_x + v_z \underline{c}_z \tag{8.9}$$

Applying coordinate transformation Equation (8.1) to Equation (8.9), we obtain

$$\underline{v}_{\mathrm{CM}} = (v_x \cos\theta + v_z \sin\theta)\,\underline{e}_x + (-v_x \sin\theta + v_z \cos\theta)\,\underline{e}_z \tag{8.10}$$

The translational kinematic equations then follow immediately from (8.8) and (8.10)

$$\dot{x} = v_x \cos\theta + v_z \sin\theta \tag{8.11}$$

$$\dot{z} = -v_x \sin\theta + v_z \cos\theta \tag{8.12}$$

The acceleration of the vehicle center of mass can be found by differentiating (8.9).

$$\begin{aligned} \underline{a} &= \dot{v}_x \underline{c}_x + \dot{v}_z \underline{c}_z + \omega_y \underline{c}_y \times (\dot{v}_x \underline{c}_x + \dot{v}_z \underline{c}_z) \\ &= (\dot{v}_x + \omega_y v_z)\, \underline{c}_x + (\dot{v}_z - \omega_y v_x)\, \underline{c}_z \end{aligned} \tag{8.13}$$

If the total external force, $\underline{F} = F_x \underline{c}_x + F_z \underline{c}_z$, applied to the vehicle is known, the translational dynamic equations are obtained from Newton's second law,

$$\dot{v}_x = -\omega_y v_z + \frac{F_x}{m} \tag{8.14}$$

$$\dot{v}_z = \omega_y v_x + \frac{F_z}{m} \tag{8.15}$$

where m is the sprung mass of the vehicle. The vehicle unsprung mass is neglected throughout this work. If it were not, the mass term in Equation (8.15) would need to be modified to account for the vehicle unsprung mass. The forces F_x and F_z will be derived later in Section 8.1.4.

8.1.3 Suspension Model

The suspension and tire assembly is modeled as shown in Figure 8.2. The spring and dashpot in the upper portion represent the suspension, while the spring in the lower portion models the tire stiffness. At any instant, the orientation of the tire spring K_w is assumed to be normal to the road surface. The tire damping behavior and its mass are neglected. The exclusion of the tire mass and its damping characteristic will allow a higher portion of high-frequency noise to pass from the road to the sprung mass. Note that the suspension height, h_i, is defined as the distance along the vehicle axis $\underline{c}_z$ measured from the tire center to the vehicle center of mass and not as the length of the spring.

In simulations where the road surface is a straight line, as seen on the left half of Figure 8.3, the relationship between the tire radius r_{w_i} and the suspension height h_i can be easily found using a geometric approach by summing all the vectors in a loop. The loop starts from the vehicle center of mass, goes to the tip of the suspension, down to the road, follows back along the road surface, and returns to the vehicle center of mass. Following

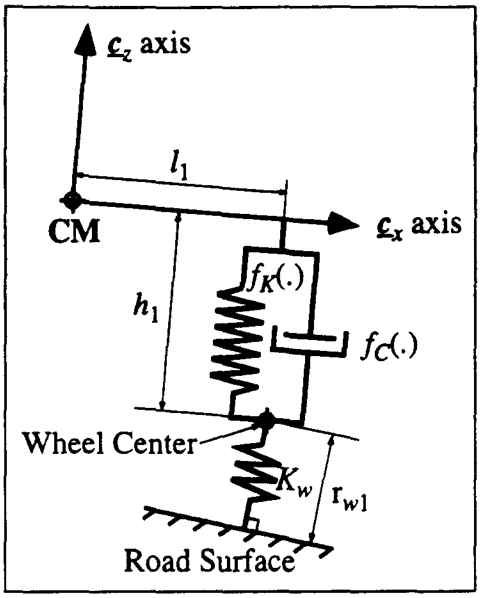

Figure 8.2: Schematic view of suspension and tire models showing the front half of the vehicle.

this path leads to:

$$[l_i \underline{c}_x - h_i \underline{c}_z - (\xi_i + r_{w_i}) \underline{r}_z - y_i \underline{r}_x + (z - b(x)) \underline{e}_z] \cdot \underline{r}_z = 0 \qquad i = \{1, 2\} \tag{8.16}$$

where l_i is the half wheelbase from the center of mass to the i^{th} wheel, ξ_i represents road variations which can be used to model bumps, potholes, road noise and any other road irregularities, and $b(x)$ is a function describing the road height at any location x. Furthermore l_i is positive whereas l_2 is negative since l_2 points in the negative $\underline{c}_x$ direction. The reason for naming the wheelbase in a vector format is that the simulation code can be written more compactly.

Using equations (8.1) and (8.2) to transform Equation (8.16), a relationship between tire radius and the suspension height is found

$$r_{w_i} + h_i \cos(\theta - \Delta) = (z - b(x)) \cos \Delta - l_i \sin(\theta - \Delta) - \xi_i \qquad i = \{1, 2\} \tag{8.17}$$

The relationship between the tire radius and the suspension height in situations involving varying road surface can be found by going around a similar loop as seen on the right half of

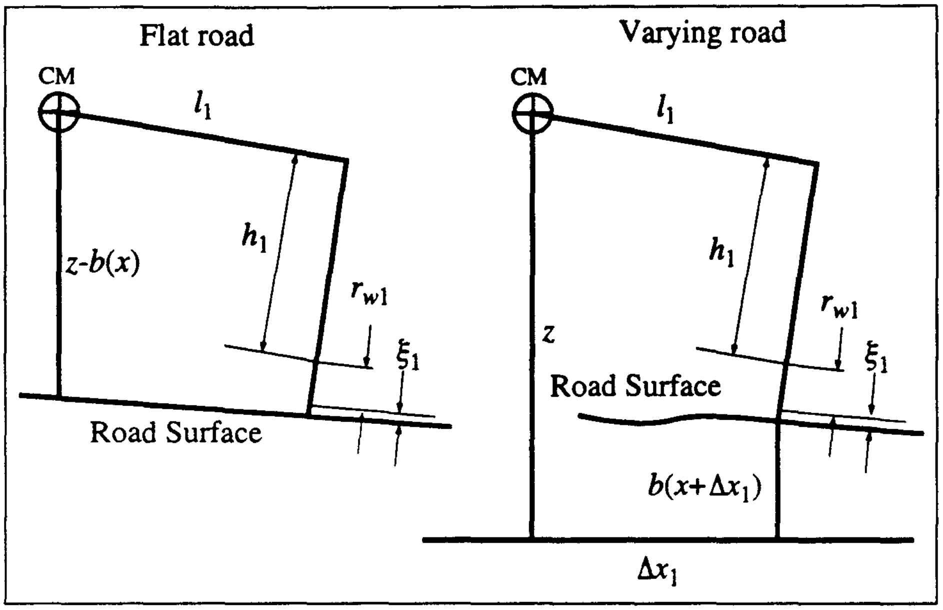

Figure 8.3: Geometric constraints involving the suspension height showing the front half of the vehicle for planar and arbitrary road surfaces.

Figure 8.3. However, solving for the suspension height requires solving a nonlinear equation,

$$l_i \underline{c}_x - h_i \underline{c}_z - (\xi_i + r_{w_i}) \underline{r}_{z_i} - b(x + \Delta x_i) \underline{e}_z - \Delta x_i \underline{e}_x + z \underline{e}_z = 0 \qquad i = \{1, 2\} \tag{8.18}$$

in which relative tire position Δx_i, the suspension height, and the wheel radius are not independent. An additional equation is required to provide a relationship between the tire radius and the suspension height in order to yield a unique solution in the equation above. This additional equation comes from a single state equation using a force balance and the assumption of a massless wheel. If the wheel is assumed to be massless, the total force applied at the center of the wheel must vanish an any direction. Consider the all the forces in the $\underline{c}_x$ direction. The tire force in the $\underline{c}_x$ direction must balance the suspension force which is generated by the suspension spring and damper. This leads to the following state equation involving the suspension height.

$$-K_w (r_{w_i} - r_{w0}) \cos(\theta - \Delta_i) = f_K(h_i) + f_C(\dot{h}_i) \qquad i = \{1, 2\} \tag{8.19}$$

where $f_K(\cdot)$ and $f_C(\cdot)$ are functions describing the force response of suspension spring and damper, respectively. These functions will be specified in the next section. Depending on the damping function, we can solve for $\dot{h}_i$ in closed-form if the function $f_C(\cdot)$ is invertible; otherwise we will have to approximate.

With the addition of Equation (8.19), Equation (8.18) now contains two unknown but dependent variables, which are the relative tire position and the wheel radius. There is no closed-formed solution to Equation (8.18) if the road surface is arbitrary.

Two methods of solving this nonlinear equation have been examined. The first approach uses a nonlinear equation solver routine to approximate the solution. The generality and flexibility of the routine supplied with MatLab^{TM} causes this application to require a prohibitively long computation time. The second approach is to exploit some of the special properties inherent in the system to make some approximations so that the relative tire position and the wheel radius can be determined. Consider the most general situation where the vehicle is traveling on an arbitrary road surface. By taking the dot product of Equation (8.18) with unit vector $\underline{e}_x$, the relative tire position can be expressed as

$$\Delta x_i = l_i \cos\theta - h_i \sin\theta - (r_{w_i} + \xi_i)\sin\Delta_i \qquad i = \{1, 2\} \tag{8.20}$$

where r_{w_i} and Δ_i are functions of x_i. It is not possible to solve this equation analytically. However, by examining the last term closely, one can make some reasonable assumptions which permit an approximate solution. First the road variation is assumed to be zero. Since the wheel stiffness constant is very high, it is reasonable to assume that the wheel radius is equal to the nominal wheel radius at equilibrium. Furthermore to eliminate the dependency of the road angle on the relative tire location, we will assume that the road angle Δ_i is approximately the same as at the position where the center of the wheel projects down to the road surface. In the worst case scenario where the road elevation is taken to be 15%, the deviation between the real location and the assumed location where the road elevation is used is at most 5 cm. This is a very small distance for the road elevation to vary significantly. Hence the solution for the relative tire position can be approximated as

$$\Delta \tilde{x}_i = l_i \cos\theta - h_i \sin\theta - r_{w_0} \sin\Delta_i \qquad i = \{1, 2\} \tag{8.21}$$

where the road angle Δ_i is evaluated at the projection of the wheel center down to the road surface. This point can be expressed as $x + l_i \cos\theta - h_i \sin\theta$.

Once the relative tire position is known, the approximate wheel radius can be obtained from Equation (8.18) by taking the dot product with unit vector $\underline{r}_{z_i}$ at the point of contact between the tire and the road surface. This leads to:

$$\tilde{r}_{w_i} = -l_i \sin(\theta - \Delta_i) - h_i \cos(\theta - \Delta_i) - \xi_i + (z - b(x + \Delta\tilde{x}_i)) \cos\Delta_i - \Delta\tilde{x}_i \sin\Delta_i, \quad i = \{1, 2\}$$

where the road angle Δ_i is evaluated at the approximated tire position.

8.1.4 Forces

The forces developed in this section include the gravitational force, aerodynamic forces, and suspension forces. The gravitational force on the vehicle is expressed as

$$\begin{aligned} \underline{F}_g &= -mg\underline{e}_z \\ &= -F_g\underline{e}_z \end{aligned} \tag{8.22}$$

When the vehicle longitudinal speed is large or high wind speed is present, air drag plays a significant role. The longitudinal drag is proportional to the square of the relative wind speed, $v_{wr} = v_w - v_x$, that is, the difference between the wind speed and vehicle speed, and has the same direction as the relative wind speed,

$$\begin{aligned} \underline{D} &= \frac{1}{2} C_D A_f \rho_a v_{wr}^2 \underline{c}_x \\ &= D\underline{c}_x \end{aligned} \tag{8.23}$$

where C_D is the drag coefficient, A_f is the vehicle effective frontal area, and ρ_a is the air density. The sign of the coefficient determines the direction of the drag force based on the direction of the relative wind speed. In addition, there is also a lift component due to the asymmetric shape of the top and bottom of the vehicle. The lift force can be described by the following equation,

$$\begin{aligned} \underline{L} &= \frac{1}{2} C_L A_f \rho_a v_{wr}^2 \underline{c}_z \\ &= L\underline{c}_z \end{aligned} \tag{8.24}$$

where C_L is the lift coefficient. These drag and lift coefficients are specific to each vehicle. However one can generalize to a class of vehicles, such as sedans, sport cars and vans. Data for these coefficients obtained by Yip *et al.* (Yip et al. 1992) for typical sedans is used in the simulation. Both the drag and lift forces are assumed to act at the vehicle center of mass.

Here the relative velocity is assumed to be negative. If it were not, equations (8.23) and (8.24) would have to be modified to account for situations where v_{wr} is positive. Furthermore, there is also a vertical wind speed component along the vehicle vertical direction, but it is ignored since the relative wind speed in this direction is small resulting in a negligible force as compared to the suspension forces.

Given the suspension height, a nonlinear function is used to model the response of the suspension spring which is governed by the following equation,

$$F_{si} = -K_{si}(h_i - h_{0i}) - \bar{K}_{si}(h_i - h_{0i})^5, \qquad i = \{1,2\} \tag{8.25}$$

where h_{0i} is the uncompressed suspension height, which can be found once the vehicle height at equilibrium is known.

The tire elastic characteristic is modeled as a linear spring having a stiffness constant K_w,

$$F_{w_i} = -K_w(r_{w_i} - r_{w_0}), \qquad i = \{1,2\} \tag{8.26}$$

where r_{w_0} is the uncompressed tire radius, assuming each tire has the same properties.

The suspension damper is modeled as piecewise linear damper having discontinuous slope at $\pm\bar{w}$ as seen in Figure 8.4,

$$F_{di} = \begin{cases} C_{di}\dot{h}_i & |\dot{h}_i| < \bar{w} \\ C_{di}\bar{w} + \bar{C}_{di}(\dot{h}_i - \bar{w}) & \dot{h}_i \geq \bar{w} \\ -C_{di}\bar{w} + \bar{C}_{di}(\dot{h}_i + \bar{w}) & \dot{h}_i \leq -\bar{w} \end{cases} \qquad i = \{1,2\} \tag{8.27}$$

where C_{di} and $\bar{C}_{di}$ specify the slope in the first and second regions, respectively.

Let the force applied at the ground by the tire at the contact point between the road surface and the tire be

$$\underline{F}_{w_i} = F_{wf_i}\underline{r}_x + N_i\underline{r}_z, \qquad i = \{1,2\} \tag{8.28}$$

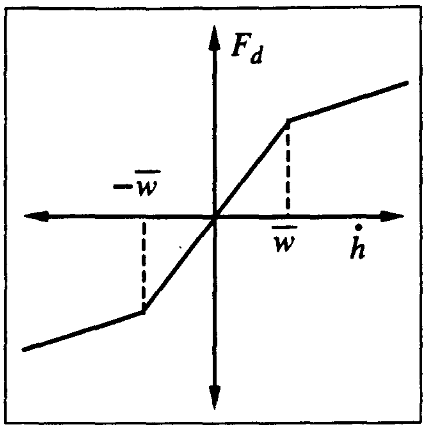

Figure 8.4: Damper characteristic.

then the road normal force, N_i, is simply the force exerted on the road by the tire.

$$N_i = -K_w(r_{w_i} - r_{w0}), \qquad i = \{1, 2\} \tag{8.29}$$

Furthermore the tire tractive force, F_{wf_i}, is a function of the normal force and the tire slip ratio. Various tire models have been formulated. The longitudinal tire model by Bakker *et al.* (Bakker et al. 1987, Bakker and Pacejka 1989) is used in the simulation discussed in Section 8.3. The tire model is described in detail in Section 8.1.8.

With the external force known, the total force acting on the vehicle is obtained by combining equations (8.22), (8.23), (8.24), (8.28) and (8.29). This leads to:

$$F_x = \sum_{i=1}^{2} [F_{wf_i} \cos(\theta - \Delta_i) + K_w(r_{w_i} - r_{w0}) \sin(\theta - \Delta_i)] + F_g \sin\theta + D \tag{8.30a}$$

$$F_z = \sum_{i=1}^{2} [F_{wf_i} \sin(\theta - \Delta_i) - K_w(r_{w_i} - r_{w0}) \cos(\theta - \Delta_i)] - F_g \cos\theta + L \tag{8.30b}$$

8.1.5 Moments About the Vehicle Center of Mass

The moment about the car center of mass is generated from two sources. The first source is from the suspension force and the second is from the aerodynamic effect due to the asymmetric shape of the vehicle. Since this section concerns pitch rotation only, only the moment about the y-axis is needed. Knowing the forces at the suspension supports and the corresponding moment arms, the moment term generated by the suspension forces is given as

$$\begin{aligned}\underline{M}_{\text{sus}} &= (l_i \underline{c}_x - h_i \underline{c}_z) \times (F_{wf_i} \underline{r}_x + N_i \underline{r}_z) \\ &= \sum_{i=1}^{2} M_{\text{sus}_i} \underline{c}_y \end{aligned} \tag{8.31}$$

where

$$M_{\text{sus}_i} = -h_i \left[F_{wf_i} \cos(\theta - \Delta_i) - N_i \sin(\theta - \Delta_i)\right] + l_i \left[F_{wf_i} \sin(\theta - \Delta_i) + N_i \cos(\theta - \Delta_i)\right]$$

The aerodynamic contribution to the moment about the car center of mass has been investigated by Yip *et al.* (Yip et al. 1992) and is given below

$$\begin{aligned}\underline{M}_w &= \frac{1}{2} C_{wy} A_f \rho_a L v_{wr}^2 \underline{c}_y \\ &= M_{wy} \underline{c}_y \end{aligned} \tag{8.32}$$

where L is the wheelbase length and the y-axis moment coefficient, C_{wy} is determined experimentally for each vehicle.

Hence the total moment applied about the car center of mass is the sum of the two moment components given above in (8.31) and (8.32).

$$\underline{M}_y = (M_{\text{sus}_1} + M_{\text{sus}_2} + M_{wy})\, \underline{c}_y \tag{8.33}$$

8.1.6 Brake Dynamics

The total brake torque, T_{ba}, applied to the wheels and the commanded brake torque, T_{bc}, are presumed to be related by the following first order lag equation,

$$\dot{T}_{ba} = \frac{T_{bc} - T_{ba}}{\tau_b} \tag{8.34}$$

where τ_b is the time delay constant which models, to the first order, the dynamics of the brake actuators and hydraulics. The total brake torque is then distributed between the front and the rear tire according to a brake biasing constant, k_b.

$$T_{b1} = k_b T_{ba} \tag{8.35a}$$

$$T_{b2} = (1 - k_b T_{ba} \tag{8.35b}$$

Each torque T_{bi} is positive and is limited to a maximum value where wheel lockup occurs. When the wheel angular velocity reaches zero, the brake torque is changed appropriately to prevent the wheel from rotating backwards.

8.1.7 Wheel Dynamics

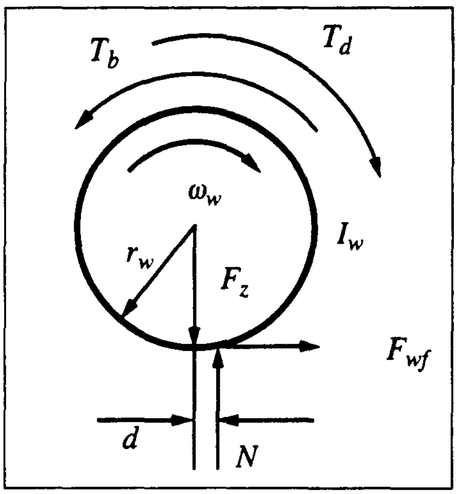

Figure 8.5: Wheel rotation.

In this model the wheels are assumed to be massless, but they are allowed to have nonzero moment of inertia I_w. Figure 8.5 shows the details of the wheel model which are used to obtain the front and rear wheel rotational dynamic equations.

$$\dot{\omega}_{w_i} = \frac{(T_{di} - r_{w_i} F_{wf_i} - d_i N_i - T_{bi})}{I_w} \qquad i = \{1, 2\} \tag{8.36}$$

The applied torques are the engine torque, T_d, and the brake torque, T_b. The road normal force, N_i, is offset to the front of the wheel by a distance d. Furthermore, the engine torque applied to each wheel is a function of the total engine output torque, T_e, which will be described in Section 8.1.9, and is distributed between the front and the rear wheels according to a drive biasing constant, k_d.

$$\begin{aligned} T_{d1} &= k_d T_e && (8.37a) \\ T_{d2} &= (1 - k_d T_e && (8.37b) \end{aligned}$$

For example, set $k_d = 1$ for front-wheel drive vehicles.

8.1.8 Tire Traction Model

The longitudinal tire tractive force, F_{wf_i}, is correlated with the tire normal force, $N_i = -K_w(r_{w_i} - r_{w0})$, and its slip ratio, λ_i, through the *Magic Formula* which was developed by Bakker and Pacejka (Bakker et al. 1987, Bakker and Pacejka 1989). This model can accurately fit experimental tire data through the use of twelve coefficients and will be described shortly.

Finding the tire slip ratio requires knowing the wheel forward velocity parallel the road surface. Let $\underline{P}_{w_i}$ be the position vector locating the wheel center,

$$\underline{P}_{w_i} = \underline{P}_{\mathrm{CM}} + l_i \underline{c}_x - h_i \underline{c}_z, \qquad i = \{1, 2\} \tag{8.38}$$

hence the wheel velocity follows by taking the inertial time derivative of the position vector $\underline{P}_{w_i}$.

$$\dot{\underline{P}}_{w_i} = (v_x - h_i \omega_y)\underline{c}_x + (v_z - l_i \omega_y - \dot{h}_i)\underline{c}_z, \qquad i = \{1, 2\} \tag{8.39}$$

The wheel forward velocity can now be found by taking the dot product with the road unit vector $\underline{r}_{xi}$.

$$\begin{aligned} v_{wf_i} &= \dot{\underline{P}}_{w_i} \cdot \underline{r}_{xi} \\ &= (v_x - h_i \omega_y)\cos(\theta - \Delta_i) + (v_z - l_i \omega_y - \dot{h}_i)\sin(\theta - \Delta_i), \qquad i = \{1, 2\} && (8.40) \end{aligned}$$

The slip ratio is defined as

$$\lambda_i = 1 - \frac{v_{wf_i}}{r_w \omega_{w_i}}, \qquad i = \{1, 2\} \tag{8.41}$$

Finally the tire tractive force can be expressed as a nonlinear function of the normal force and slip ratio.

$$F_{wf_i} = f(N_i, \lambda_i), \qquad i = \{1,2\} \tag{8.42}$$

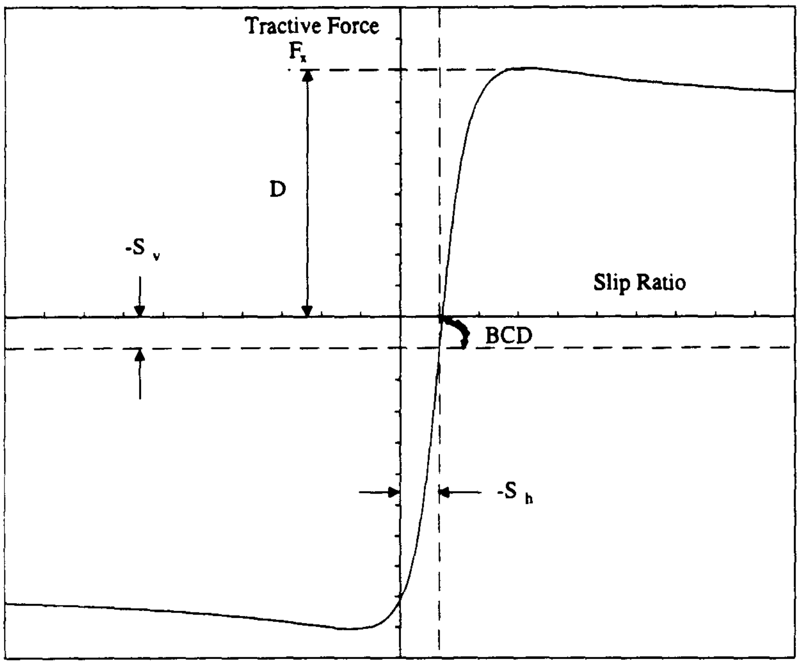

Figure 8.6: Exaggerated plot of the *Magic Formula*, showing the influence of the coefficients.

As mentioned above, Bakker (Bakker et al. 1987, Bakker and Pacejka 1989) proposes the following *Magic Formula* to fit the tire tractive force numerically. This formula has been shown to accurately fit experimental tire data and has the form

$$y(x) = D \sin\left(C \tan^{-1}\left(Bx - E\left[Bx - \tan^{-1}(Bx)\right]\right)\right) \tag{8.43}$$

with

$$x = \lambda + S_h \tag{8.44a}$$

$$f(N, \lambda) = y(x) + S_v \tag{8.44b}$$

Figure 8.6, a plot of the tractive force versus the slip ratio, shows the physical meaning of the coefficients in Equations (8.43) and (8.44). Since the tractive force is also a function of the normal force, these coefficients may be related to the normal force with following quantities.

$$D = a_1 N^2 + a_2 N \tag{8.45a}$$

$$BCD = (a_3 N^2 + a_4 N) \exp^{-a_5 N} \tag{8.45b}$$

$$C = a_0 \tag{8.45c}$$

$$E = a_6 N^2 + a_7 N + a_8 \tag{8.45d}$$

$$B = BCD/CD \tag{8.45e}$$

$$S_h = a_9 N + a_{10} \tag{8.45f}$$

$$S_v = a_{11} \tag{8.45g}$$

Once the experimental data for tire tractive force of a specific tire is collected, the quantities a_0 to a_{11} can be obtained using various curve-fitting techniques.

8.1.9 Engine Model

A simple engine model taken from Smith and Starkey (Smith and Starkey 1992) is used here. The output torque T_e, is a function of the engine speed ω_e, gear ratio ζ, drive train efficiency η, and throttle position TP. Thus,

$$T_e = \mathrm{TP}\zeta\eta\left[c_1\left(\frac{\omega_e}{100}\right)^2 + c_2\left(\frac{\omega_e}{100}\right) + c_3\right] \tag{8.46}$$

By choosing the coefficients c_1, c_2, and c_3, engine torque curves can be closely approximated. For a manual transmission, the engine speed is given by

$$\omega_e = \zeta\omega_{w1} \quad \text{front-wheel drive} \tag{8.47}$$

$$\omega_e = \zeta\omega_{w2} \quad \text{rear-wheel drive} \tag{8.48}$$

The range of TP is between zero, for no output torque, and one, for maximum torque output at a certain engine speed. In addition, the actual throttle position response to the commanded throttle position is modeled as a first order lag,

$$\dot{\mathrm{TP}} = \frac{(\mathrm{TP}_c - \mathrm{TP})}{\tau_t} \tag{8.49}$$

where τ_t is the throttle delay time constant.

8.2 Nonlinear Lateral and Longitudinal Model

The full six degree of freedom model includes longitudinal, lateral and vertical translations and roll, pitch and yaw rotations. Including kinematic relations, the system of equations is 12^{th} order. Development of the six degree of freedom model closely follows the derivation where motion is restricted to the vertical plane. Subcomponents from the longitudinal model are generalized to the full nonlinear model and a steering system and road noise model are added.

8.2.1 Reference Frames

Using the longitudinal model as the stepping stone, we now can proceed to explore the complex behavior of the vehicle's lateral and longitudinal dynamics. As seen before, the first step is to define all the reference frames, which consist of the Earth-fixed frame, the vehicle-fixed frame, and the four road frames associated with the four tires.

First the Earth-fixed reference frame E with origin $\mathcal{O}$ as seen in Figure 8.7 is defined with unit vectors $(\underline{e}_x, \underline{e}_y, \underline{e}_z)$. A second frame C fixed in the vehicle with origin at the vehicle center of mass is defined with unit vectors $(\underline{c}_x, \underline{c}_y, \underline{c}_z)$. As seen in Figure 8.8 this frame C may be described by three successive rotations from frame E. First rotate the Earth-fixed frame about $\underline{e}_z$ axis by an amount ε, which is known as yaw angle. This leads to frame A with unit vectors $(\underline{a}_x, \underline{a}_y, \underline{a}_z)$. Next rotate frame A about $\underline{a}_x$ by an amount ϕ to obtain intermediate frame B with unit vectors $(\underline{b}_x, \underline{b}_y, \underline{b}_z)$. This angular rotation is called the roll angle. Finally rotate frame B about $\underline{b}_y$ by an angular displacement θ, which is the pitch

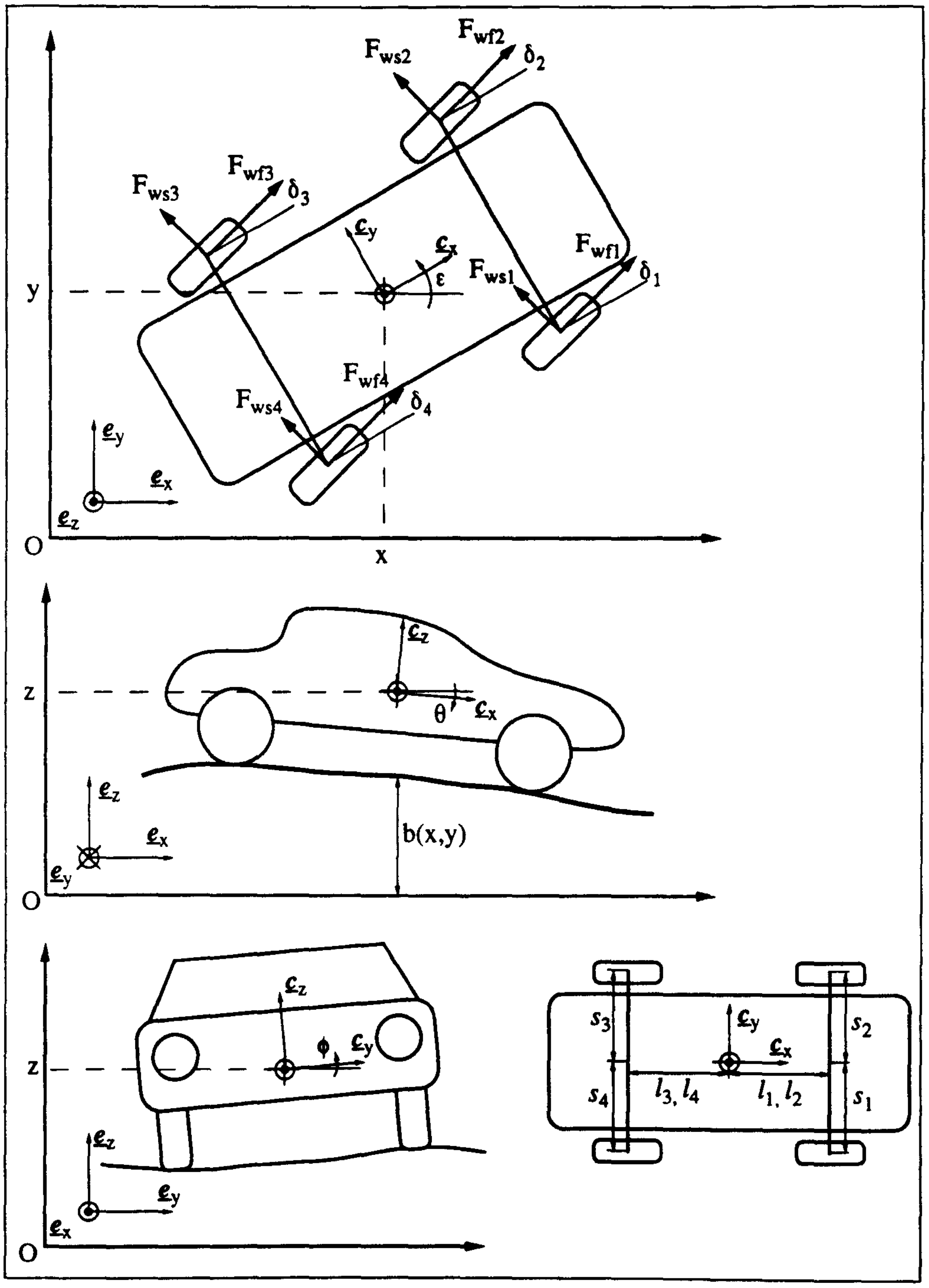

Figure 8.7: Representation of nonlinear vehicle model.

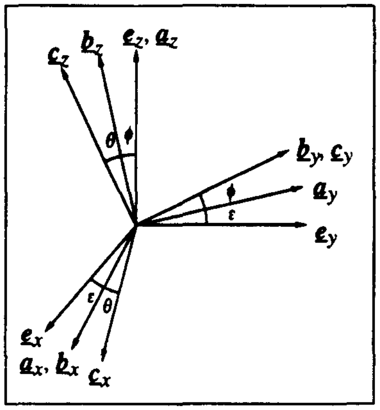

Figure 8.8: Relationship between reference frames.

angle, to obtain the vehicle-fixed frame C. The corresponding coordinate transformation matrices are given below:

$$\begin{bmatrix} \underline{a}_x \\ \underline{a}_y \\ \underline{a}_z \end{bmatrix} = \begin{bmatrix} \cos\varepsilon & \sin\varepsilon & 0 \\ -\sin\varepsilon & \cos\varepsilon & 0 \\ 0 & 0 & 1 \end{bmatrix} \begin{bmatrix} \underline{e}_x \\ \underline{e}_y \\ \underline{e}_z \end{bmatrix} \tag{8.50}$$

$$\begin{bmatrix} \underline{b}_x \\ \underline{b}_y \\ \underline{b}_z \end{bmatrix} = \begin{bmatrix} 1 & 0 & 0 \\ 0 & \cos\phi & \sin\phi \\ 0 & -\sin\phi & \cos\phi \end{bmatrix} \begin{bmatrix} \underline{a}_x \\ \underline{a}_y \\ \underline{a}_z \end{bmatrix} \tag{8.51}$$

$$\begin{bmatrix} \underline{c}_x \\ \underline{c}_y \\ \underline{c}_z \end{bmatrix} = \begin{bmatrix} \cos\theta & 0 & -\sin\theta \\ 0 & 1 & 0 \\ \sin\theta & 0 & \cos\theta \end{bmatrix} \begin{bmatrix} \underline{b}_x \\ \underline{b}_y \\ \underline{b}_z \end{bmatrix} \tag{8.52}$$

Now the transformation matrix from unit vectors in E to unit vectors in C reference frame can be readily determined as:

$$\begin{bmatrix} \underline{c}_x \\ \underline{c}_y \\ \underline{c}_z \end{bmatrix} = \begin{bmatrix} \cos\theta & 0 & -\sin\theta \\ 0 & 1 & 0 \\ \sin\theta & 0 & \cos\theta \end{bmatrix} \begin{bmatrix} 1 & 0 & 0 \\ 0 & \cos\phi & \sin\phi \\ 0 & -\sin\phi & \cos\phi \end{bmatrix} \begin{bmatrix} \cos\varepsilon & \sin\varepsilon & 0 \\ -\sin\varepsilon & \cos\varepsilon & 0 \\ 0 & 0 & 1 \end{bmatrix} \begin{bmatrix} \underline{e}_x \\ \underline{e}_y \\ \underline{e}_z \end{bmatrix} \tag{8.53}$$

In addition, the inverse of the above transformation matrix is its transpose.

The road reference frame R with unit vectors $(\underline{r}_x, \underline{r}_y, \underline{r}_z)$ for each tire is defined with the origin located at the point of contact between the tire and the road surface. As shown in Figure 8.9, the orientation of this frame R is such that the $\underline{r}_z$ component coincides with the road normal vector, which is specified at each tire location (x, y) and is given as

$$\underline{n} = n_x\underline{e}_x + n_y\underline{e}_y + n_z\underline{e}_z$$

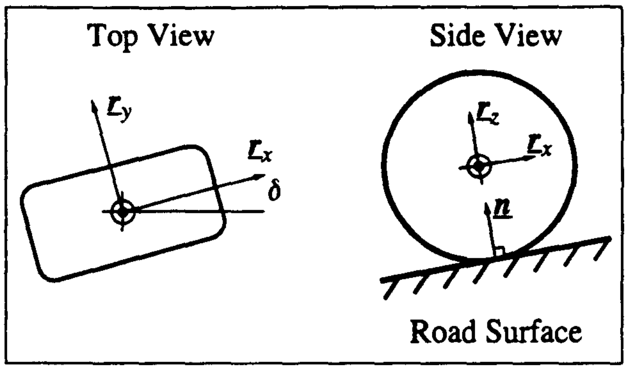

Figure 8.9: Definition of road frame.

Using the transpose of the transformation matrix of Equation (8.53), the $\underline{r}_z$ component can be expressed in the vehicle-fixed reference frame as:

$$\underline{r}_z = r_{zx}\underline{c}_x + r_{zy}\underline{c}_y + r_{zz}\underline{c}_z \tag{8.54}$$

where

$$r_{xx} = n_x(\cos\varepsilon\cos\theta - \sin\varepsilon\sin\phi\sin\theta) + n_y(\sin\varepsilon\cos\theta + \cos\varepsilon\sin\phi\sin\theta) - n_z\cos\phi\sin\theta \tag{8.55}$$

$$r_{xy} = -n_x\sin\varepsilon\cos\phi + n_y\cos\varepsilon\cos\phi + n_z\sin\phi \tag{8.56}$$

$$r_{xz} = n_x(\cos\varepsilon\sin\theta + \sin\varepsilon\sin\phi\cos\theta) + n_y(\sin\varepsilon\sin\theta - \cos\varepsilon\sin\phi\cos\theta) + n_z\cos\phi\cos\theta \tag{8.57}$$

A second unit vector $\underline{r}_x$ of frame R is chosen such that it is normal to the tire axis of rotation and points in the direction of the tire heading.

Let $\underline{r}_x$ be expressed as

$$\underline{r}_x = r_{xx}\underline{c}_x + r_{xy}\underline{c}_y + r_{xz}\underline{c}_z$$

the components of $\underline{r}_x$ can be found by noting that

$$\underline{r}_x \cdot (-\sin\delta\underline{c}_x + \cos\delta\underline{c}_y) = 0 \tag{8.58a}$$

$$\underline{r}_z \cdot \underline{r}_x = 0 \tag{8.58b}$$

$$\|\underline{r}_x\| = 1 \tag{8.58c}$$

We can use the first property in Equation (8.58) to solve for r_{xy} in terms of r_{xx} and the tire steering angle.

$$r_{xy} = r_{xx} \tan\delta \tag{8.59}$$

Invoking the second property in Equation (8.58) and Equation (8.59) to solve for r_{xz} in terms of r_{xx} and the known components of $\underline{r}_z$, leads to the following equation:

$$r_{xz} = -\frac{r_{zx} + r_{zy}\tan\delta}{r_{zz}} r_{xx} \tag{8.60}$$

Note that r_{zz} can never be zero because it would mean that the road surface is vertical with respect to the vehicle body. Finally we can use the third property in Equation (8.58), that is, $r_{xx}^2 + r_{xy}^2 + r_{xz}^2 = 1$ and Equations (8.59) and (8.60) to solve for r_{xx} as:

$$r_{xx} = \frac{1}{\sqrt{1 + \tan^2\delta + \left(\frac{r_{zx}+r_{zy}\tan\delta}{r_{zz}}\right)^2}} \tag{8.61}$$

Hence the solutions for r_{xy} and r_{xz} follow directly from equations (8.59), (8.60) and (8.61).

$$r_{xy} = \frac{\tan\delta}{\sqrt{1 + \tan^2\delta + \left(\frac{r_{zx}+r_{zy}\tan\delta}{r_{zz}}\right)^2}} \tag{8.62}$$

$$r_{xz} = \frac{r_{zx} + r_{zy}\tan\delta}{r_{zz}\sqrt{1 + \tan^2\delta + \left(\frac{r_{zx}+r_{zy}\tan\delta}{r_{zz}}\right)^2}} \tag{8.63}$$

Then reference frame R is completely specified based on the right-handed orthogonal axis system and the third unit vector is given by $\underline{r}_y = \underline{r}_z \times \underline{r}_x$. Hence the unit vectors of the road frame can be expressed compactly in terms of the vehicle-fixed unit vectors as:

$$\begin{bmatrix} \underline{r}_x \\ \underline{r}_y \\ \underline{r}_z \end{bmatrix} = \begin{bmatrix} r_{xx} & r_{xy} & r_{xz} \\ r_{yx} & r_{yy} & r_{yz} \\ r_{zx} & r_{zy} & r_{zz} \end{bmatrix} \begin{bmatrix} \underline{c}_x \\ \underline{c}_y \\ \underline{c}_z \end{bmatrix} \tag{8.64}$$

Furthermore if it may be assumed that each tire lies on an independent road surface, then a subscript i is added. Subscripts $i = \{1, 2, 3, 4\}$ refer to front right, front left, rear left, and rear right tires respectively.

8.2.2 Vehicle Dynamics

The dynamic equations of motion are derived from Newton's law applied in an inertial reference frame. The rotational dynamics are derived first. The translational dynamics follow.

Rotational Equations of Motion

With the angular rotations defined above, the angular velocity of the vehicle is given by:

$$\underline{\omega} = \dot{\varepsilon}\underline{e}_z + \dot{\phi}\underline{a}_x + \dot{\theta}\underline{b}_y \tag{8.65}$$

Use the coordinate transformation matrices in (8.50) through (8.52) to obtain the vehicle angular velocity in the vehicle-fixed coordinate frame as

$$\begin{aligned}\underline{\omega} &= (\dot{\phi}\cos\theta - \dot{\varepsilon}\cos\phi\sin\theta)\underline{c}_x + (\dot{\theta} + \dot{\varepsilon}\sin\phi)\underline{c}_y + (\dot{\phi}\sin\theta + \dot{\varepsilon}\cos\phi\cos\theta)\underline{c}_z \\ &= \omega_x\underline{c}_x + \omega_y\underline{c}_y + \omega_z\underline{c}_z \end{aligned} \tag{8.66}$$

Solving for $\dot{\varepsilon}$, $\dot{\phi}$ and $\dot{\theta}$, the rotational kinematic equations of motion are:

$$\dot{\varepsilon} = \frac{1}{\cos\phi}(-\sin\theta\omega_x + \cos\theta\omega_z) \tag{8.67a}$$

$$\dot{\phi} = \cos\theta\omega_x + \sin\theta\omega_z \tag{8.67b}$$

$$\dot{\theta} = \tan\phi(\sin\theta\omega_x - \cos\theta\omega_z) + \omega_y \tag{8.67c}$$

Furthermore the rotational dynamic equations are obtained from Euler's equations.

$$\dot{\omega}_x = \frac{M_x}{I_x} + \omega_y\omega_z\frac{I_y - I_z}{I_x} \tag{8.68a}$$

$$\dot{\omega}_y = \frac{M_y}{I_y} + \omega_z\omega_x\frac{I_z - I_x}{I_y} \tag{8.68b}$$

$$\dot{\omega}_z = \frac{M_z}{I_z} + \omega_x\omega_y\frac{I_x - I_y}{I_z} \tag{8.68c}$$

where M_x, M_y and M_z, which will be derived later in Section 8.2.5, are the total moment applied about the ($\underline{c}_x$, $\underline{c}_y$ and $\underline{c}_z$) axes resulting from the suspension and aerodynamic interactions, and I_x, I_y and I_z are the moments of inertia of the sprung mass about the $(\underline{c}_x, \underline{c}_y, \underline{c}_z)$ axes, respectively. The unsprung mass is neglected in this work.

Translational Equations of Motion

Let $\underline{P}_{\mathrm{CM}} = x\underline{e}_x + y\underline{e}_y + z\underline{e}_z$ be the position vector from the Earth-fixed origin $\mathcal{O}$ to the vehicle center of mass as seen in Figure 8.7. Then the velocity of the mass center can be expressed either in Earth-fixed or vehicle-fixed coordinates as

$$\begin{aligned} \underline{v}_{\mathrm{CM}} &= \dot{x}\underline{e}_x + \dot{y}\underline{e}_y + \dot{z}\underline{e}_z && (8.69) \\ &= v_x\underline{c}_x + v_y\underline{c}_y + v_z\underline{c}_z && (8.70) \end{aligned}$$

Applying Equation (8.53) to transform Equation (8.70) into an Earth-fixed frame leads to

$$\begin{aligned} &\underline{v}_{\mathrm{CM}} = \\ &\quad [v_x(\cos\varepsilon\cos\theta - \sin\varepsilon\sin\phi\sin\theta) - v_y\sin\varepsilon\cos\phi + v_z(\cos\varepsilon\sin\theta + \sin\varepsilon\sin\phi\cos\theta)]\,\underline{e}_x + \\ &\quad [v_x(\sin\varepsilon\cos\theta + \cos\varepsilon\sin\phi\sin\theta) + v_y\cos\varepsilon\cos\phi + v_z(\sin\varepsilon\sin\theta - \cos\varepsilon\sin\phi\cos\theta)]\,\underline{e}_y + \\ &\quad [-v_x\cos\phi\sin\theta + v_y\sin\phi + v_z\cos\phi\cos\theta]\,\underline{e}_z && (8.71) \end{aligned}$$

Hence the translational kinematic equations follow immediately from (8.69) and (8.71).

$$\begin{aligned} \dot{x} &= v_x(\cos\varepsilon\cos\theta - \sin\varepsilon\sin\phi\sin\theta) - v_y\sin\varepsilon\cos\phi + \\ &\quad v_z(\cos\varepsilon\sin\theta + \sin\varepsilon\sin\phi\cos\theta) && (8.72a) \\ \dot{y} &= v_x(\sin\varepsilon\cos\theta + \cos\varepsilon\sin\phi\sin\theta) + v_y\cos\varepsilon\cos\phi + \\ &\quad v_z(\sin\varepsilon\sin\theta - \cos\varepsilon\sin\phi\cos\theta) && (8.72b) \\ \dot{z} &= -v_x\cos\phi\sin\theta + v_y\sin\phi + v_z\cos\phi\cos\theta && (8.72c) \end{aligned}$$

The acceleration of the vehicle center of mass can be found by differentiating (8.70).

$$\begin{aligned} \underline{a} &= \dot{v}_x\underline{c}_x + \dot{v}_y\underline{c}_y + \dot{v}_z\underline{c}_z + (\omega_x\underline{c}_x + \omega_x\underline{c}_x + \omega_x\underline{c}_x) \times (\omega_x\underline{c}_x + \omega_x\underline{c}_x + \omega_x\underline{c}_x) \\ &= (\dot{v}_x + \omega_y v_z - \omega_z v_y)\underline{c}_x + (\dot{v}_y + \omega_z v_x - \omega_x v_z)\underline{c}_y + (\dot{v}_z + \omega_x v_y - \omega_y v_x)\underline{c}_z && (8.73) \end{aligned}$$

If the total external force applied to the vehicle is known,

$$\underline{F} = F_x\underline{c}_x + F_y\underline{c}_y + F_z\underline{c}_z$$

the translational dynamic equations are obtained from Newton's second law,

$$\dot{v}_x = \omega_z v_y - \omega_y v_z + \frac{F_x}{m} \tag{8.74a}$$

$$\dot{v}_y = \omega_x v_z - \omega_z v_x + \frac{F_y}{m} \tag{8.74b}$$

$$\dot{v}_z = \omega_y v_x - \omega_x v_y + \frac{F_z}{m} \tag{8.74c}$$

where m is the sprung mass of the vehicle. The forces are derived in Section 8.2.4.

8.2.3 Suspension Model

The suspension model for lateral and longitudinal vehicle motion is similar in every aspect to the longitudinal model. The extension to the three dimensional model slightly changes the geometric constraint equation corresponding to Equation (8.18) and is given below for the most general case,

$$\begin{aligned} 0 \;=\; & l_i \underline{c}_x - s_i \underline{c}_y - h_i \underline{c}_z - b(x + \Delta x_i, y + \Delta y_i)\underline{e}_z - (r_{w_i} + \xi_i)\underline{r}_{z_i} - \Delta x_i \underline{e}_x - \Delta y_i \underline{e}_y + z\underline{e}_z, \\ & i = \{1, 2, 3, 4\} \end{aligned} \tag{8.75}$$

where l_i is the half wheelbase from the vehicle center of mass to the i^{th} wheel, s_i is the half track width from the vehicle center of mass to the i^{th} wheel, Δx_i and Δy_i are the relative tire distances from the center of mass to the i^{th} wheel, and the function $b(x, y)$ describes the road surface at location (x, y).

Solving for the relationship between r_{w_i} and h_i requires solving a nonlinear equation. In the special case where the road surface is planar, it is possible to solve for the relationship between the tire radius and the suspension height analytically as in the longitudinal model.

$$r_{w_i} + h_i r_{zz} = [z - b(x, y)]\, n_z + l_i r_{zx} - s_i r_{zy} - \xi_i, \qquad i = \{1, 2, 3, 4\} \tag{8.76}$$

In addition four state equations governing the suspension height at four wheels are needed:

$$-K_w(r_{w_i} - r_{w_0}) \cos(\theta - \Delta_i) = f_K(f_i + f_C(\dot{h}_i), \qquad i = \{1, 2, 3, 4\} \tag{8.77}$$

As stated in Section 8.1.3, solving for $\dot{h}_i$ depends on the damping function $f_C(\cdot)$.

To solve for the wheel radius and the relative tire position for an arbitrary road surface, requires making some approximations. Using the same concept as in Section 8.1.3, first approximate the relative tire position which is denoted by Δx_i and Δy_i. These two relative tire position locators can be found by taking the dot product of Equation (8.75) with unit vectors $\underline{e}_x$ and $\underline{e}_x$ respectively. This leads to:

$$\begin{aligned}
\Delta x_i &= l_i(\cos\varepsilon\cos\theta - \sin\varepsilon\sin\phi\sin\theta) + s_i\sin\varepsilon\cos\phi - \\
&\quad h_i(\cos\varepsilon\sin\theta + \sin\varepsilon\sin\phi\cos\theta) - (r_{w_i} + \xi_i)n_{x_i}, \qquad i = \{1,2,3,4\} \\
\Delta y_i &= l_i(\sin\varepsilon\cos\theta + \cos\varepsilon\sin\phi\sin\theta) + s_i\cos\varepsilon\cos\phi - \\
&\quad h_i(\sin\varepsilon\sin\theta + \cos\varepsilon\sin\phi\cos\theta) - (r_{w_i} + \xi_i)n_{y_i}, \qquad i = \{1,2,3,4\} \quad (8.78)
\end{aligned}$$

Following the same approach in Section 8.1.3, assume that the road variation is zero, the wheel radius is constant, and the road normal vector is evaluated at the point where wheel center projects down to the road surface. This leads to the following equations where the relative tire position locators can be approximated as:

$$\begin{aligned}
\Delta\tilde{x}_i &= l_i(\cos\varepsilon\cos\theta - \sin\varepsilon\sin\phi\sin\theta) + s_i\sin\varepsilon\cos\phi - \\
&\quad h_i(\cos\varepsilon\sin\theta + \sin\varepsilon\sin\phi\cos\theta) - r_{w0}n_{x_i}, \qquad i = \{1,2,3,4\} \qquad (8.79) \\
\Delta\tilde{y}_i &= l_i(\sin\varepsilon\cos\theta + \cos\varepsilon\sin\phi\sin\theta) + s_i\cos\varepsilon\cos\phi - \\
&\quad h_i(\sin\varepsilon\sin\theta + \cos\varepsilon\sin\phi\cos\theta) - r_{w0}n_{y_i}, \qquad i = \{1,2,3,4\} \qquad (8.80)
\end{aligned}$$

Once the tire location is approximated, the wheel radius can be found by taking the dot product of Equation (8.75) with unit vector $\underline{r}_{z_i}$, leading to:

$$\begin{aligned}
\tilde{r}_{w_i} &= l_i z_{zx_i} - s_i r_{zy_i} - h_i r_{zz_i} - \xi_i - \Delta\tilde{x}_i n_{x_i} - \Delta\tilde{y}_i n_{y_i} + [z - b(x + \Delta\tilde{x}_i, y + \Delta\tilde{y}_i)]\, n_{z_i}, \\
&\quad i = \{1,2,3,4\} \qquad (8.81)
\end{aligned}$$

where the quantities n_{x_i}, n_{y_i} and n_{z_i} are evaluated at the approximated tire location $(x + \Delta\tilde{x}_i, y + \Delta\tilde{y}_i)$.

8.2.4 Forces

The gravitational force on the vehicle is $\underline{F}_g = -mg\underline{e}_z$. In addition to longitudinal wind lift and drag forces,

$$\begin{aligned} \underline{L} &= \frac{1}{2}C_L A_f \rho_a v_{wr}^2 \underline{e}_z \\ \underline{D} &= \frac{1}{2}C_D A_f \rho_a v_{wr}^2 \underline{e}_x \end{aligned}$$

there is now a lateral wind component which comes from crosswinds, large passing vehicles or fast lateral maneuvers. Moreover, these wind forces may have a considerable effect on lateral vehicle dynamics. This side force is modeled here as:

$$\begin{aligned} \underline{F}_s &= \frac{1}{2}C_S A_f \rho_a v_{wr}^2 \underline{e}_y && \text{(8.82a)} \\ &= F_s \underline{e}_y && \text{(8.82b)} \end{aligned}$$

Work by Yip *et al.* (Yip et al. 1992) has correlated the force coefficients C_L, C_D and C_Y to the relative wind speed and its angle relative to the vehicle longitudinal axis. These two variables are shown in Figure 8.10, and the analytical expressions for β and v_{wr} are given as:

$$\begin{aligned} v_{wr} &= \sqrt{(v_{wx} - v_x)^2 + (v_{wy} - v_y)^2} && \text{(8.83)} \\ \beta &= \tan^{-1}\left(\frac{v_{wy} - v_y}{v_{wx} - v_x}\right) && \text{(8.84)} \end{aligned}$$

Let the force applied to each tire by the road be expressed as

$$\underline{F}_{w_i} = F_{wf_i}\underline{r}_x + F_{ws_i}\underline{r}_y + N_i\underline{r}_z$$

where the tire tractive and side force are obtained from the tire model in Section 8.2.7 and the tire normal force is simply

$$N_i = -K_w(r_{w_i} - r_{w0})$$

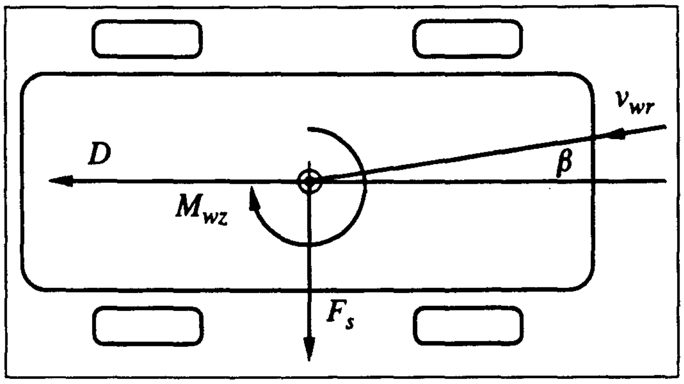

Figure 8.10: Aerodynamic forces acting on the vehicle have three components.

Then the force components applied to the vehicle along its three principal axes $(\underline{c}_x, \underline{c}_y, \underline{c}_z)$ can be expressed as:

$$F_x = \sum_{i=1}^{4}[F_{wf_i}r_{xx} + F_{ws_i}r_{yx} - K_w(r_{w_i} - r_{w0})r_{zx}] + F_g\cos\phi\sin\theta + D \quad (8.85)$$

$$F_y = \sum_{i=1}^{4}[F_{wf_i}r_{xy} + F_{ws_i}r_{yy} - K_w(r_{w_i} - r_{w0})r_{zy}] - F_g\sin\phi + F_S \quad (8.86)$$

$$F_z = \sum_{i=1}^{4}[F_{wf_i}r_{xz} + F_{ws_i}r_{yz} - K_w(r_{w_i} - r_{w0})r_{zz}] - F_g\cos\phi\cos\theta + L \quad (8.87)$$

8.2.5 Moments About the Vehicle Center of Mass

Aerodynamics also contributes to the moment about the vehicle center of mass. Work by Yip *et al.* (Yip et al. 1992) has correlated the aerodynamic moment to the relative wind speed. The moment equation has a form similar to the aerodynamic force equation and is given below in vector form,

$$\underline{M}_w = \frac{1}{2}\rho_a v_{wr}^2 A_f L(C_{wx}\underline{c}_x + C_{wy}\underline{c}_y + C_{wz}\underline{c}_z) \quad (8.88a)$$

$$= M_{wx}\underline{c}_x + M_{wy}\underline{c}_y + M_{wz}\underline{c}_z \quad (8.88b)$$

where L is the wheel base length, and the moment coefficients C_{wx}, C_{wy} and C_{wz} can be correlated to the relative wind speed and its angle in equations (8.83) and (8.84).

The total moment about the center of mass, which is contributed by the suspension forces and the aerodynamic forces, is obtained below:

$$\underline{M} = \sum_{i=1}^{4}(l_i\underline{c}_x - s_i\underline{c}_y - h_i\underline{c}_z) \times (F_{wf_i}\underline{r}_x + F_{ws_i}\underline{r}_y + N_i\underline{r}_z) + \underline{M}_w \tag{8.89}$$

Decomposing the moment equation into the three components about the vehicle principal axes using Equation (8.53) leads to the following moment equations.

$$M_x = \sum_{i=1}^{4} M_{x_i} + M_{wx} \tag{8.90a}$$

$$M_y = \sum_{i=1}^{4} M_{y_i} + M_{wy} \tag{8.90b}$$

$$M_z = \sum_{i=1}^{4} M_{z_i} + M_{wz} \tag{8.90c}$$

where

$$M_{x_i} = (F_{wf_i}(-s_i r_{xz_i} + h_i r_{xy_i}) + F_{ws_i}(-s_i r_{yz_i} + h_i r_{yy_i}) - K_w(r_{w_i} - r_{w0})(-s_i r_{zz_i} + h_i r_{zy_i}))$$

$$M_{y_i} = (F_{wf_i}(-l_i r_{xz_i} + h_i r_{xx_i}) + F_{ws_i}(l_i r_{yz_i} + h_i r_{yx_i}) - K_w(r_{w_i} - r_{w0})(l_i r_{zz_i} + h_i r_{zx_i}))$$

$$M_{z_i} = (F_{wf_i}(l_i r_{xy_i} + s_i r_{xx_i}) + F_{ws_i}(l_i r_{yy_i} + s_i r_{yx_i}) - K_w(r_{w_i} - r_{w0})(l_i r_{zy_i} + s_i r_{zx_i}))$$

8.2.6 Brake Dynamics

The brake dynamics are modeled as a first order lag similar to that used in the longitudinal model. The total brake torque T_{ba} is distributed between the front and the rear wheels according to a brake biasing constant k_b and is evenly divided between the left and the right wheels.

$$\begin{array}{lllll} T_{b1} & = T_{b2} & = \frac{k_b}{2}T_{ba} & & \text{front wheels} \\ T_{b3} & = T_{b4} & = \frac{(1-k_b)}{2}T_{ba} & & \text{rear wheels} \end{array} \tag{8.91}$$

Again T_{bi} is positive and is limited to a maximum value which is where wheel lockup occurs.

8.2.7 Wheel Dynamics and Tire Traction Model

The wheel dynamics are the same as that of the longitudinal model, however the tire traction model requires an additional variable since a lateral force and self-aligning moment are present. This additional variable is known as the lateral slip angle α and is defined below. In Bakker's nonlinear tire model (Bakker et al. 1987, Bakker and Pacejka 1989, Pacejka and Bakker 1991), the tire tractive force, side force and self-aligning moment are functions of the normal force, the tire longitudinal slip ratio, and lateral slip angle. In order to find the tire tractive, side force and self-aligning moment, define the longitudinal slip and the slip angle. The longitudinal slip is defined in the same way as in the longitudinal model, that is,

$$\lambda_i = 1 - \frac{v_{wf_i}}{r_{w_i}\omega_{w_i}}, \qquad i = \{1,2,3,4\} \tag{8.92}$$

The wheel forward velocity v_{wf_i} can be found by first finding the velocity at the center of the tire.

$$\begin{aligned} \underline{\dot{P}}_{w_i} &= (v_x - h_i\omega_y + s_i\omega_z)\underline{c}_x + (v_y + h_i\omega_x + l_i\omega_z)\underline{c}_y + (v_z - l_i\omega_y - s_i\omega_x - \dot{h}_i)\underline{c}_z, \\ & \quad i = \{1,2,3,4\} \end{aligned} \tag{8.93}$$

Using Equation (8.64) we can transform Equation (8.93) to the road reference frame and the wheel forward velocity follows directly.

$$\begin{aligned} v_{w_i} &= (v_x - h_i\omega_y + s_i\omega_z)r_{xx_i} + (v_y + h_i\omega_x + l_i\omega_z)r_{xy_i} + (v_z - l_i\omega_y - s_i\omega_x - \dot{h}_i)r_{xz_i}, \\ & \quad i = \{1,2,3,4\} \end{aligned} \tag{8.94}$$

The tire slip angle as seen in Figure 8.11 is defined as the angle between the wheel velocity vector and the wheel heading vector. Thus,

$$\begin{aligned} \alpha_i &= \delta_i - \tan\left(\frac{v_{wy}}{v_{wx}}\right) \\ &= \delta_i - \tan\left(\frac{v_y + h_i\omega_x + l_i\omega_z}{v_x - h_i\omega_y + s_i\omega_z}\right), \qquad i = \{1,2,3,4\} \end{aligned} \tag{8.95}$$

where δ_i is the steering angle of each wheel.

The tractive force, side force and self-aligning moment can now be expressed as nonlinear functions of the tire normal force, slip ratio, slip angle, and other variables such as road surface conditions, and camber angle. The camber angle is defined as the inclination of

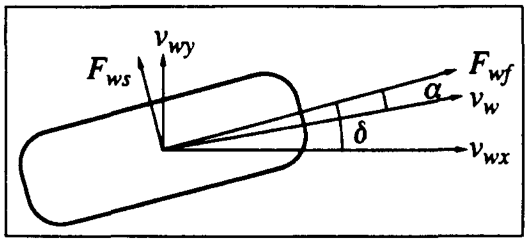

Figure 8.11: Top view of a tire under steering maneuver.

	Brake Force	**Side Force**	**Self-aligning Moment**
D	$a_1N^2 + a_2N$	$b_1N^2 + b_2$	$c_1N^2 + c_2N$
BCD	$(a_3N^2 + a_4N)\exp^{-a_5N}$	$[b_3 \sin(b_4 \tan^{-1}(b_5N))] \cdot (1 - b_{12}\gamma)$	$(c_3N^2 + c_4N)\exp^{-c_5N} \cdot (1 - c_{12}\|\gamma\|)$
C	a_0	b_0	a_0
E	$a_6N^2 + a_7N + a_8$	$b_6N^2 + b_7N + b_8$	$4\frac{a_6N^2+a_7N+a_8}{1-c_{13}\|\gamma\|}$
B	BCD/CD	BCD/CD	BCD/CD
S_h	$a_9N + a_{10}$	$b_9\gamma$	$a_9\gamma$
S_v	a_{11}	$(b_{10}N^2 + b_{11}N)\gamma$	$(a_{10}N^2 + a_{11}N)\gamma$

Table 8.1: Tire model coefficients.

the wheel plane from a plane perpendicular to the road surface and parallel to the vehicle longitudinal axis.

The general formulation of the tire model developed by Bakker *et al.* has the form:

$$y(x) = D\sin\left(C\tan^{-1}\left(Bx - E\left[Bx - \tan^{-1}(Bx)\right]\right)\right) \tag{8.96}$$

with

$$x = X + S_h \tag{8.97a}$$

$$Y(X) = y(x) + S_v \tag{8.97b}$$

where the variable $Y(X)$ represents either the tire tractive force, side force or self-aligning moment, and the variable X represents the corresponding slip ratio or slip angle. The coefficients above may be related to the tire normal force and camber angle γ as in Table 8.1. The above formulations are developed in cases of pure traction or pure cornering maneuvers. When the vehicle experiences a combination of cornering and braking, equations relating the tractive force, side force and self-aligning moment to the slip quantities require modification. Bakker (Bakker et al. 1987, Bakker and Pacejka 1989, Pacejka and Bakker 1991) provides the following method. First, define normalized slip quantities as follows:

$$\lambda^* = \frac{\lambda}{\lambda_{\text{max}}} \tag{8.98}$$

$$\alpha^* = \frac{\alpha}{\alpha_{\text{max}}} \tag{8.99}$$

where λ_{max} and α_{max} are values where the tractive and side forces, respectively, reach a maximum. Next define the correction factor σ^* as:

$$\sigma^* = \sqrt{(\lambda^*)^2 + (\alpha^*)^2} \tag{8.100}$$

The modified equations for the tractive force, side force and self-aligning moment can be expressed as:

$$F_x = \frac{\lambda}{\sigma^*} F_{x_0}(\sigma^*, N) \tag{8.101}$$

$$F_y = \frac{\alpha^*}{\sigma^*} F_{y_0}(\sigma^*, N) \tag{8.102}$$

$$M_z = \frac{\alpha^*}{\sigma^*} M_{z_0}(\sigma^*, N) \tag{8.103}$$

where F_{x_0}, F_{y_0} and M_{z_0} are functions that provide the tractive force, side force and self-aligning moment as obtained from pure traction or pure cornering.

8.2.8 Engine Model

The same engine model described in Section 8.1.9 is used to develop the full six degree of freedom vehicle model. Since this model consists of four tires instead of two, the front and rear torque is divided evenly between the left and the right tires, resulting in the following equations:

$$\begin{array}{lllll} T_{d1} & = T_{d2} & = \frac{k_d}{2} T_e & & \text{front wheels} \\ T_{d3} & = T_{d4} & = \frac{(1-k_d)}{2} T_e & & \text{rear wheels} \end{array} \tag{8.104}$$

8.2.9 Steering Model

The type of steering model implemented in this work is a fixed-control steering model. With this model, the angular displacement of the steering wheel is specified. The other type of steering model is the free-control steering system in which the torque applied to the steering wheel is specified. This type of steering model is more complex since the steering angular displacement must be solved as a function of the resultant moments and the current angular displacement of the steering wheel. As shown in Figure 8.12, the steering system is modeled as a lumped mass system described in Lukowski *et al.* (Lukowski et al. 1990). The governing equation for the front-wheel steering system is given below,

$$\ddot{\delta} = -\frac{C_{ws}}{2I_{ws}}\dot{\delta} + \frac{K_{ws}}{2I_{ws}}(\delta_c - \delta) + \frac{K_{wp}(F_{wf1} - F_{wf2}) + M_{sa}}{2I_{ws}} \tag{8.105}$$

where δ_c is the commanded angular displacement of the steering wheel, I_{ws} is the moment of inertia of front wheels about their steering axis, K_{ws} and C_{ws} are the steering rotational stiffness and damping constants, M_{sa} is the total self-aligning moment of the front wheels, and K_{wp} is the steering axis offset.

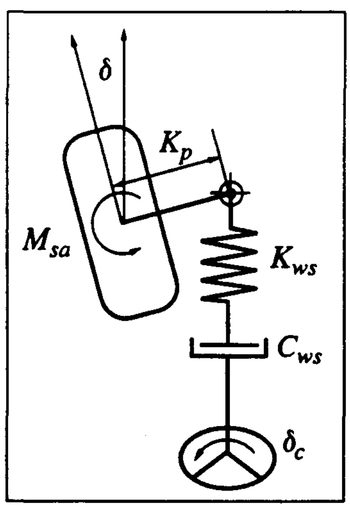

Figure 8.12: Lumped-mass representation of the steering system.

8.2.10 Random Road Excitation Model

One method of introducing random road excitation to the vehicle simulation is to generate a road noise profile at every point prior to the simulation. Such a method is developed by Cebon *et al.* (Cebon and Newland 1983) using Fourier transform methods to generate a two dimensional random road surface. However this approach is impractical, since it requires storage of enormous amounts of data. A more efficient and elegant method is to generate random road excitation on-line. With this scheme, the need to store all the road noise data is eliminated except for a small segment used to correlate the noise input between the front and the rear wheels. The method used here uses a first-order shaping filter approach and is developed by Gill (Gill 1983).

The idea behind this approach is to shape the spectral density of first order processes driven by stationary Gaussian white noise to closely approximate the measured road spectral density. Another important road characteristic besides the spectral density of the tracks, is the correlation between the left and right tracks. In order to achieve the above properties, the road noise at the left and the right wheels can be expressed as functions of two uncorrelated random processes ξ_M and θ_M.

$$\begin{bmatrix} \eta_1 \\ \eta_2 \end{bmatrix} = \begin{bmatrix} 1 & s_1 \\ 1 & s_2 \end{bmatrix} \begin{bmatrix} \xi_M \\ \theta_M \end{bmatrix} \tag{8.106}$$

The variable ξ_M describes the random road excitation at the point coinciding with the center of mass between the left and right tracks. The variable θ_M describes the noise difference between the left and the right tracks. The constants s_1 and s_2 are the half track widths from the car center to the left and right wheels respectively. Note that the constant s_1 is negative since it points in the negative $\underline{c}_y$ direction.

The random processes ξ_M and θ_M are first order processes driven by white noise.

$$\begin{bmatrix} \dot{\xi}_M \\ \dot{\theta}_M \end{bmatrix} = v_x \begin{bmatrix} \gamma_1 & 0 \\ 0 & \gamma_2 \end{bmatrix} \begin{bmatrix} \xi_M \\ \theta_M \end{bmatrix} + v_x \begin{bmatrix} \sigma_1 & 0 \\ 0 & \sigma_2 \end{bmatrix} \begin{bmatrix} w_1 \\ w_2 \end{bmatrix} \tag{8.107}$$

By specifying the constants γ_1, γ_2, σ_1 and σ_2, random road excitation may be generated with spectral density and correlation functions closely matching the experimentally measured data. Furthermore, the the constants σ_1 and σ_2 may be redefined as functions of more physically meaningful constants, for example,

$$\sigma_1 = \sqrt{S_0 2\pi(1+\alpha)} \tag{8.108a}$$

$$\sigma_2 = \sigma_1 s_2 \sqrt{\alpha} \tag{8.108b}$$

where S_0 is the spectral intensity constant and α is the coherence constant. The values of the coherence constant range from zero to one, where a value of zero indicates that there is no correlation between the left and the right tracks and a value of one indicates that the two tracks are completely correlated. For vehicles traveling straight ahead at a constant speed v_x, the random road noise at the rear wheels is that of the front wheels delayed by a time interval $t_d = \frac{l}{v_x}$. The road noise at the rear wheels can be expressed as functions of the front wheels as follows:

$$\begin{bmatrix} \eta_3(t) \\ \eta_4(t) \end{bmatrix} = \begin{bmatrix} \eta_1(t-t_d) \\ \eta_2(t-t_d) \end{bmatrix} \tag{8.109}$$

8.3 Simulation Results

8.3.1 Longitudinal Model

Response of Vehicle to Various Inputs

In this section, the longitudinal model is subjected to various inputs and its responses are examined. Figure 8.13 shows the vehicle speed and pitch angle in response to a step throttle input when the vehicle is initially traveling at $10\frac{\text{m}}{\text{sec}}$. As expected, the vehicle should pitch upward, translating to a negative pitch angle in the simulation, when the vehicle is accelerating. As time passes, the vehicle pitches downward slowly as the vehicle acceleration decreases and speed increases. The reason for this behavior is that the moment caused by the wind about the y-axis dominates at high speed and low acceleration. This moment tends to pitch the car downward as a consequence of the asymmetric design of the vehicle top and bottom. The three jumps apparent in the plot of the pitch angle, occur when the lower gear switches to higher gear. This creates a discontinuity in engine output torque, which causes the vehicle to jerk.

After holding half-throttle for 60 seconds, the throttle is released and a step brake input is applied for the next 15 seconds. Figure 8.14 shows the plots of the vehicle speed and pitch angle as a total of 1000 N of brake force is applied to the wheels. The applied torque is about 10% of the maximum torque required to lock up the wheels, assuming a skidding coefficient of friction of 0.7. As expected, the vehicle pitches down as it decelerates, corresponding to a positive pitch angle. Again the small jumps in the pitch angle plot indicate the discontinuity of engine output torque due to the gear changes before the throttle position reaches zero.

The vehicle is then simulated while traveling on an inclined road surface. There is no throttle or brake input to the vehicle. Figure 8.15 shows the plots of the vehicle pitch angle and speed when coasting down a 5% grade road. The vehicle speeds up as a result of the gravitational force. The oscillations in the pitch angle plot reflect the fact that the vehicle is not initially at equilibrium. The pitch angle plotted is referenced to the Earth-fixed horizontal axis. The difference between the pitch angle and the angle of the road is known as the relative pitch angle, a measurement of the vehicle pitch relative to the road surface. As mentioned previously, this relative pitch angle does not vanish at steady state since there is a wind generated moment about the vehicle center of mass when the vehicle is traveling at high speed.

Next, a road disturbance is modeled. The vehicle is driven over a sharp sinusoidal bump 0.01 meters high and 0.3 meters wide while traveling at $27\frac{\mathrm{m}}{\mathrm{sec}}$. The responses of the vehicle height and pitch angle are plotted in Figure 8.16. The first sharp *corner* in the pitch angle plot indicates the point where the front wheel reaches the bump and the second sharp *corner* follows when the rear wheel passes over the bump. Looking at the vehicle height, one can conclude that this is a reasonable response of the vehicle since a well maintained vehicle with good shocks should not oscillate more than once or twice when it is disturbed from equilibrium.

Finally, random road excitation is added to the front and the rear wheels. Since the vehicle is traveling along a straight path, the road noise at the rear wheel is that of the front wheel delayed by the time interval required for the rear wheel to reach to the former location of the front wheel. If the vehicle is traveling at a constant speed v_x, the delay time can be expressed as $t_d = \frac{l}{v_x}$, where l is the distance between the front and the rear wheels. The vehicle height, pitch angle, and random road input at the front wheels are plotted in Figure 8.17 while the vehicle is traveling at $27\frac{m}{sec}$. As seen in the plot of the vehicle height and the noise amplitude, the suspension system filters out the high frequency noise but passes through the low frequency components of the noise. From the plot of the pitch angle, one can also conclude that the pitch angle is more susceptible than the vehicle height to high frequency noise, even thought it also does some filtering out of the high frequency components. In addition, the simulated spectral density of the random noise process obtained by averaging 100 realizations is plotted with the theoretical spectral density in Figure 8.18. This random road excitation is typical of rough highway roads.

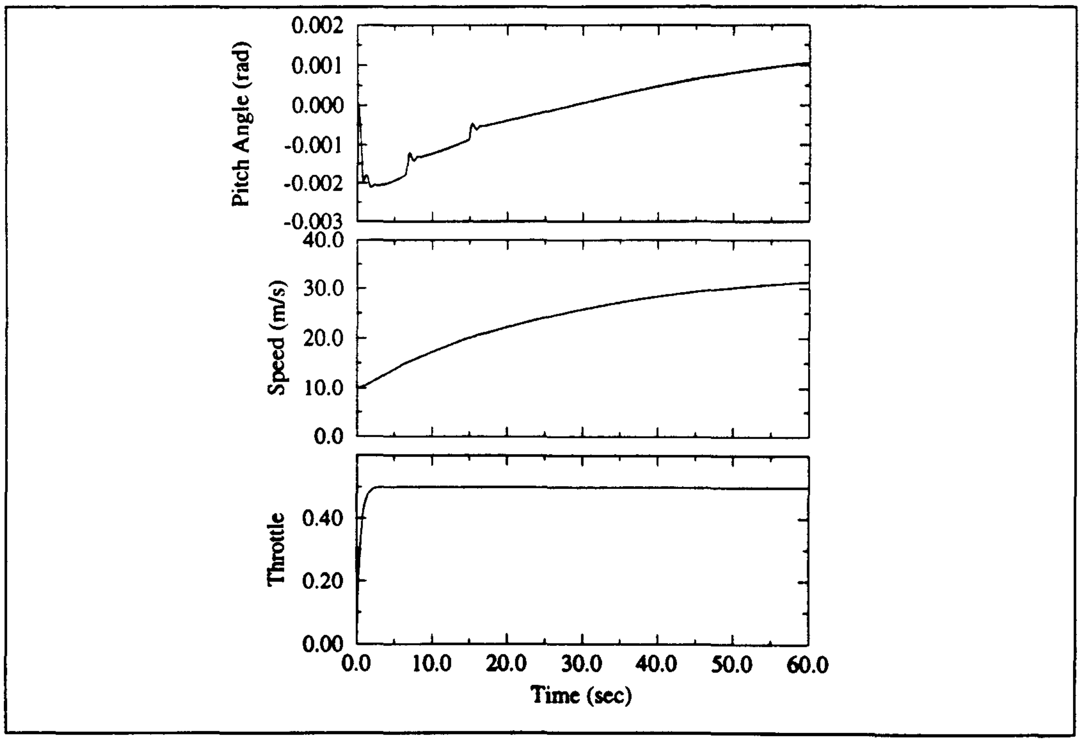

Figure 8.13: Vehicle response due to a step throttle input.

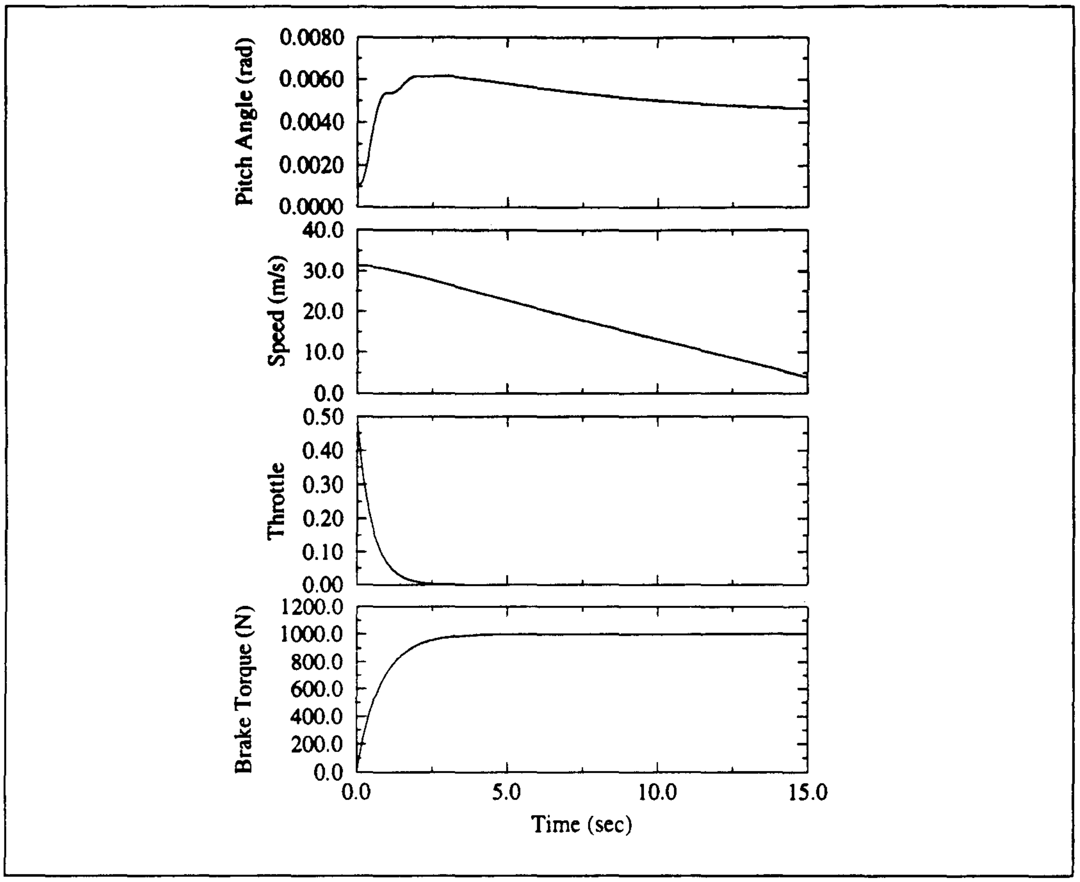

Figure 8.14: Vehicle response due to a step brake input subsequent to a step throttle input.

Small Angle Approximation

In steady-state, the magnitude of the pitch angle relative to the road surface, that is, $\theta - \Delta$, is at most on the order of 10^{-3} radian. The reason that the pitch angle does not vanish is because there is a moment about the vehicle center of mass caused by the wind at high speed. Furthermore, the maximum pitch angle relative to the road surface during a transient response of the vehicle is on the order of 10^{-2} radian. Since the relative pitch angle is small, we can make a first order approximation of the trigonometric functions without degrading the model accuracy. For any angle x, the small angle approximation of $\cos(x)$ is taken as one and that of $\sin(x)$ is taken as x. In the operating range of the pitch angle whose magnitude is less than 10^{-2} radian, the maximum error resulted from

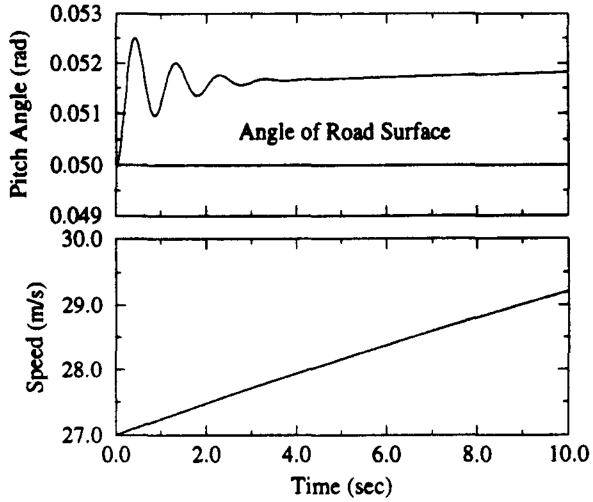

Figure 8.15: Vehicle response when decending down a 5% grade road.

making small angle approximations is less than 0.1 percent. This is too small an error to have any significant effect on the simulation accuracy. To verify this, the approximated and non-approximated systems are simulated by initially setting the relative pitch angle to a maximum value, which is taken to be 0.05 radian. The responses of the states of the approximated and non-approximated systems are compared for any significant deviations. As seen in Figure 8.19, there is no notable difference between the original model and the one using small angle approximations.

Knowing that making a small angle approximation on the relative pitch angle does not reduce the simulation accuracy, we would also like to investigate the consequences of making an approximation on the absolute pitch angle, which is referenced from the Earth-fixed horizontal axis. This might reduce the simulation accuracy if the elevation of the road is large, since the absolute pitch angle is the sum of the road angle and the vehicle pitch angle relative to the road. According to transportation literature, a typical road grade limit for highways is around 10 to 15 percent. To take a worst case scenario, we will use a maximum road grade of 15% and a maximum relative pitch angle of 0.05 radian as used previously. This will constrain the maximum limit of the absolute pitch angle to about 0.2

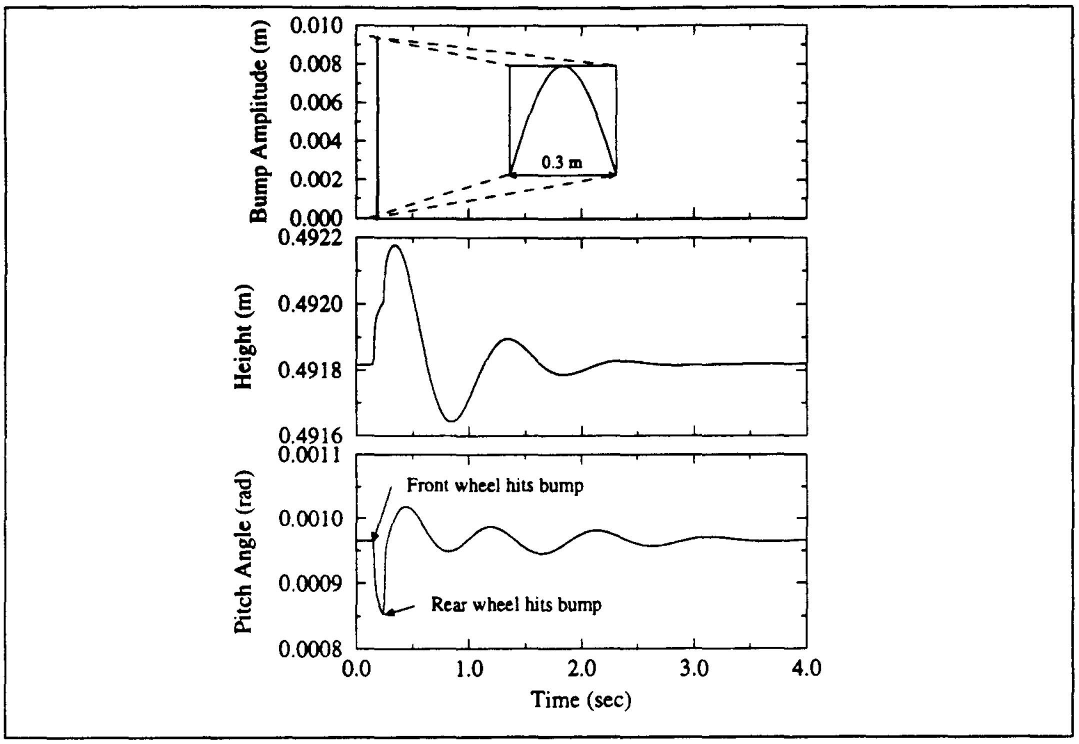

Figure 8.16: Vehicle response when passing over a sinusoidal bump.

radian. Setting the road elevation to the maximum allowable limit of 15% and the absolute pitch angle to 0.2 radians, the vehicle is simulated as it is initially traveling at $27\frac{\text{m}}{\text{sec}}$ with the nominal throttle position of 22.555% of the maximun throttle position. Comparing the response of the approximated system to the non-approximated system, we found that there are no significant deviations between the two models. The deviation in all states is below two orders of magnitude. Figure 8.20 shows the vehicle pitch angle and velocity as well as the longitudinal velocity. There are no visible differences between the approximated and non-approximated systems.

In conclusion, it is permissible to use a small angle approximation on the pitch angle. By making a small angle approximation, we can save about 5 percent in computational time. The reason that the computational gain is not significant is because we only save one multiplication operation for each cosine term. For each sine term, we still have to use one multiplication operation regardless of whether we make a small angle approximation or not.

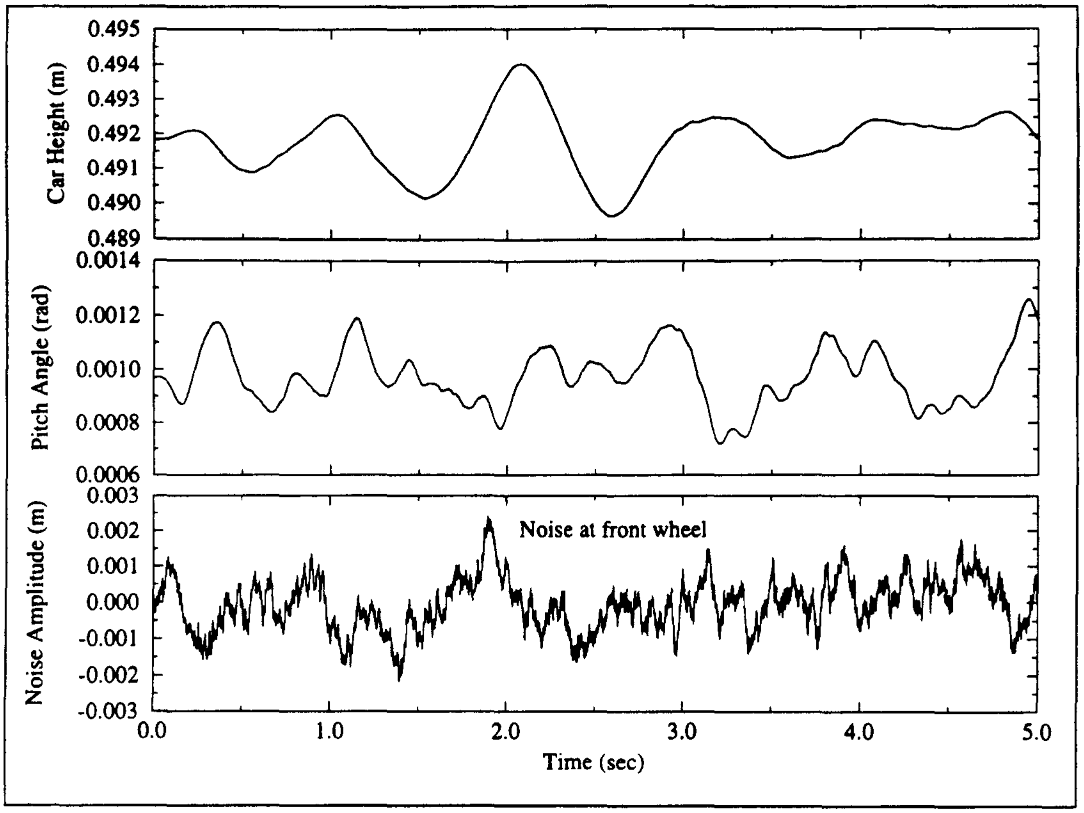

Figure 8.17: Vehicle response due to random road excitation.

Linearization at a Nominal Operating Point

A linear model of the vehicle operating at some nominal point (x_0, u_0), where $\underline{f}(x_0, u_0) = \underline{0}$, is needed to implement the fault detection and identification filter. Due to the complexity of the nonlinear model, it is impractical to linearize the system analytically. Therefore the linearized system is obtained numerically. The process to linearize the system numerically is described below.

First, a nominal operating point needs to be specified where the linearized model is obtained. This nominal point can be found by specifying the inputs and simulating the system to reach steady state. It takes about 300 seconds for the system to reach steady state. After obtaining the nominal operating point, a numerical linearization process can be implemented to obtain the linearized model.

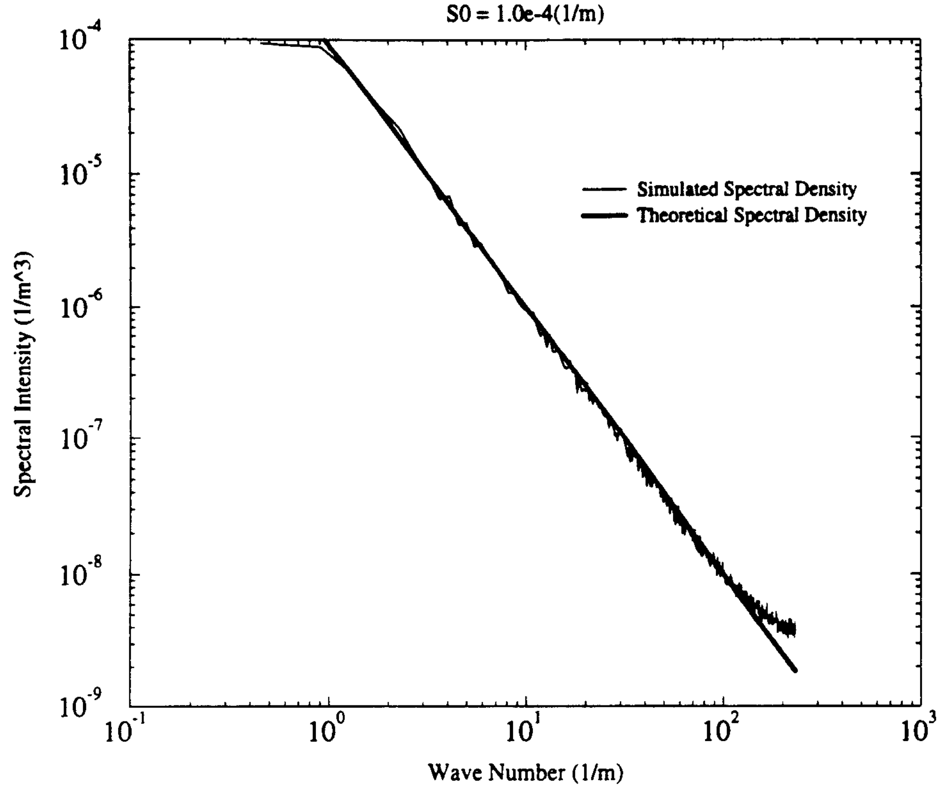

Figure 8.18: Power spectral densities of simulated and theoretical random noise processes.

Starting with the nonlinear system $\dot{\underline{x}} = \underline{f}(\underline{x}, \underline{u})$, one would like to linearize this system at some nominal point (x_0, u_0). Using Taylor's expansion, one can expand the nonlinear system around with $\underline{x} = \underline{x}_0 + \tilde{\underline{x}}$ and $\underline{u} = \underline{u}_0 + \tilde{\underline{u}}$ as

$$\dot{\tilde{\underline{x}}} = \underline{f}(\underline{x}_0, \underline{u}_0) + \nabla_{\underline{x}} \underline{f}(\underline{x}, \underline{u}) \Big|_{\substack{\underline{x} = \underline{x}_0 \\ \underline{u} = \underline{u}_0}} \tilde{\underline{x}} + \nabla_{\underline{u}} \underline{f}(\underline{x}, \underline{u}) \Big|_{\substack{\underline{x} = \underline{x}_0 \\ \underline{u} = \underline{u}_0}} \tilde{\underline{u}} + \text{higher order terms}$$

By neglecting the higher order terms and noting that $\underline{f}(x_0, u_0)$ vanishes, the linearized system becomes

$$\dot{\tilde{\underline{x}}} = A\tilde{\underline{x}} + B\tilde{\underline{u}}$$

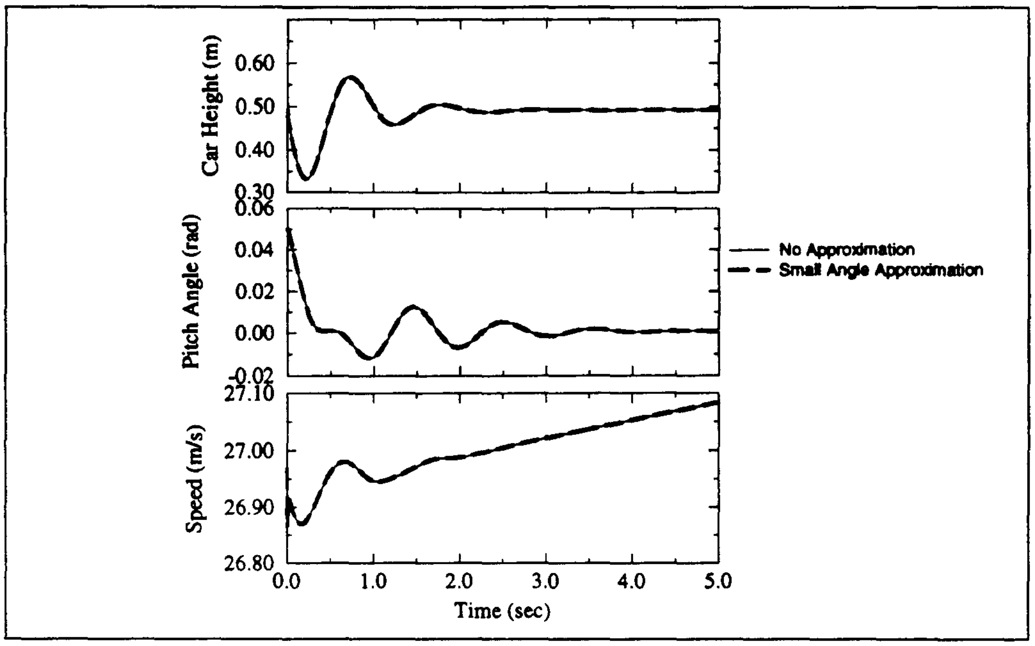

Figure 8.19: Effect of making a small angle approximation of the relative pitch angle.

$$
\begin{aligned}
A &= \underline{\nabla_x f}(\underline{x}, \underline{u}) \mid_{\substack{\underline{x} = \underline{x}_0 \\ \underline{u} = \underline{u}_0}} \\
B &= \underline{\nabla_u f}(\underline{x}, \underline{u}) \mid_{\substack{\underline{x} = \underline{x}_0 \\ \underline{u} = \underline{u}_0}}
\end{aligned}
$$

As mentioned previously, analytically calculating the gradient of the nonlinear system is impractical. Therefore an approximation scheme will be used.

Using the central difference method, the A and B matrix coefficients are approximated as

$$
\begin{aligned}
a_{ij} &= \frac{\partial f_i}{\partial x_j} \mid_{\substack{\underline{x} = \underline{x}_0 \\ \underline{u} = \underline{u}_0}} \simeq \frac{f_i(\underline{x}_0 + [\delta x]_j, \underline{u}_0) - f_i(\underline{x}_0 - [\delta x]_j, \underline{u}_0)}{2\delta x} \\
b_{ij} &= \frac{\partial f_i}{\partial u_j} \mid_{\substack{\underline{x} = \underline{x}_0 \\ \underline{u} = \underline{u}_0}} \simeq \frac{f_i(\underline{x}_0, \underline{u}_0 + [\delta u]_j) - f_i(\underline{x}_0, \underline{u}_0 - [\delta u]_j)}{2\delta x}
\end{aligned}
$$

where the notation $[\delta x]_j$ denotes a vector with zero elements everywhere except for the j^{th} element which has the value δx.

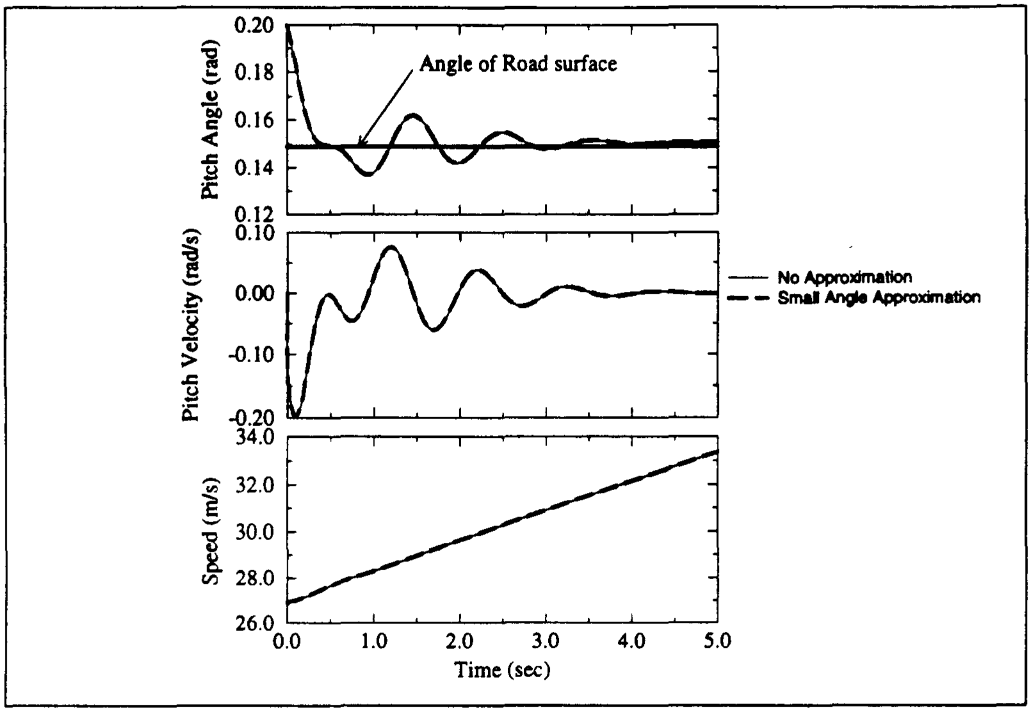

Figure 8.20: Effect of making a small angle approximation of the absolute pitch angle.

Care must be taken in choosing the perturbation values δx and δu. Truncation errors due to finite significant digits in digital computers will result if perturbation size is too small; whereas error produced by nonlinearities will result if the perturbation size is too large. Each coefficient should be plotted versus the perturbation size and each coefficient should be chosen individually within the region where the curve remains flat. Figure 8.21 shows a typical plot of one coefficient versus perturbation size in which the curve can be characterized by three regions. In region I, errors are induced by finite computer word length and indicate that the perturbation size is too small. In region III, errors are induced by model nonlinearities and indicate that the perturbation size is too large. The most accurate representation of each coefficient lies in region II where the error curve is flat. In our experience, typical values for the normalized perturbation sizes of $\frac{\delta x}{x_0}$ and $\frac{\delta u}{u_0}$ range from 10^{-6} to 10^{-3} for the central differences method.

The system is linearized at a highway speed of $27\frac{\mathrm{m}}{\mathrm{sec}}$ or 65mph. To maintain at this

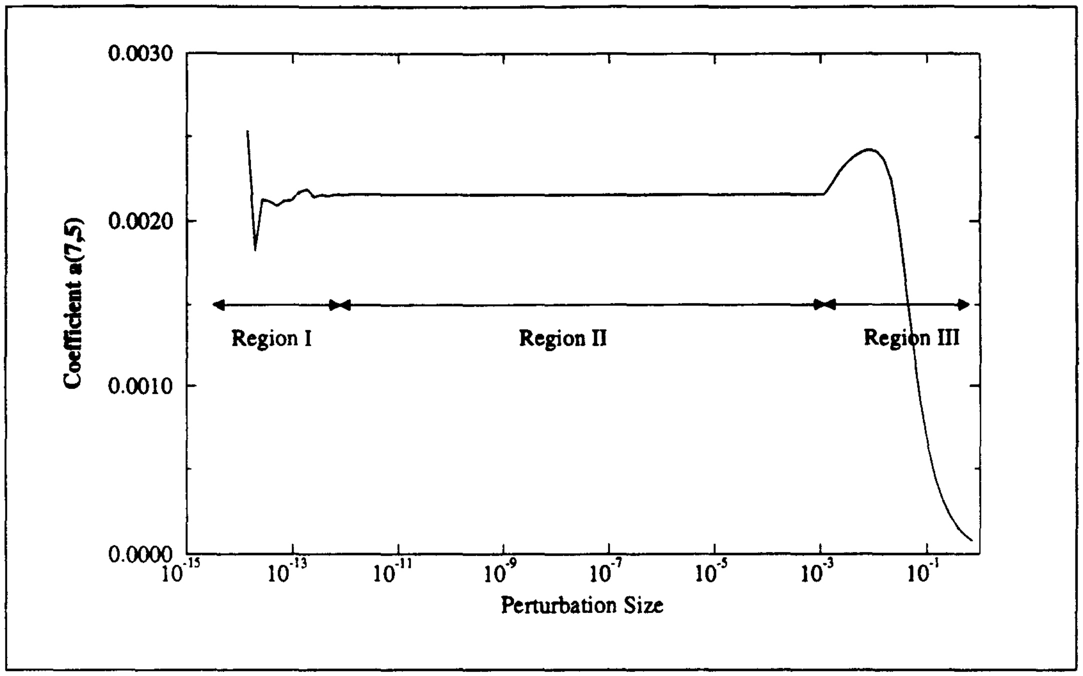

Figure 8.21: Effect of perturbation size on numerical derivative computation.

speed, the throttle position is set at 22.555% of the maximum throttle position. Figure 8.22 shows the transient responses of the vehicle when the throttle input is perturbed upward by 15 percent. The responses of the linearized system match very well to those of the nonlinear system. In addition, the vehicle steady-state responses are plotted in Figure 8.23. However, the steady state responses of the linearized system deviate from the nonlinear model considerably for large perturbations. By comparing all of the states of the linearized and nonlinear systems, we found that deviation errors between the linearized and nonlinear systems at steady state are below 10 percent for a 15 percent increase or 15 percent decrease in throttle position input. This corresponds to a range of speed from $25.5\frac{m}{sec}$ to $28.5\frac{m}{sec}$. Furthermore the brake input is also perturbed to compare the accuracy of the linearized model to that of the nonlinear model. Figure 8.24 shows that the maximum perturbation size for the brake input is 34 N such that the deviation errors of the states between the two models are less than 10 percent. As evident in the plots, the responses of the system to a brake perturbation are much more linear than those due to a throttle perturbation.

This is not surprising since the brake torque is related to the brake input through a linear first order dynamics; whereas the engine torque is not only controlled by throttle position but is also a nonlinear function of the wheel speed. If we eliminate the engine model and specify the engine torque directly, the deviation errors between the two models are less than 3 percent for the same range of speed.

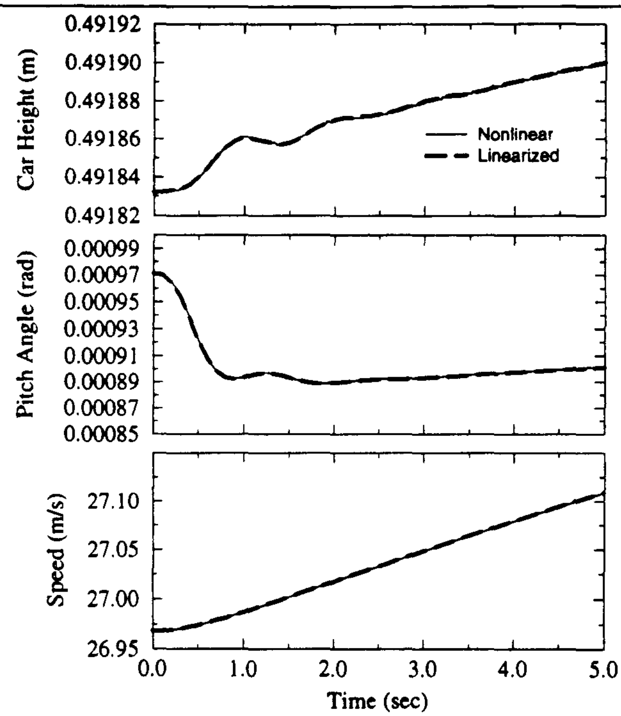

Figure 8.22: Transient response of the linearized and nonlinear systems with a perturbed throttle input (+15%).

8.3.2 Lateral and Longitudinal Model

Response of Vehicle to Various Inputs

The longitudinal response of the vehicle was analyzed in Section 8.3.1, therefore it is only necessary to investigate the vehicle lateral modes at this point. First the vehicle is stimulated with a step steering input of 0.01 radian while the vehicle is initially traveling at $27 \frac{m}{sec}$ at its corresponding nominal throttle position of 22.555% of maximum throttle position.

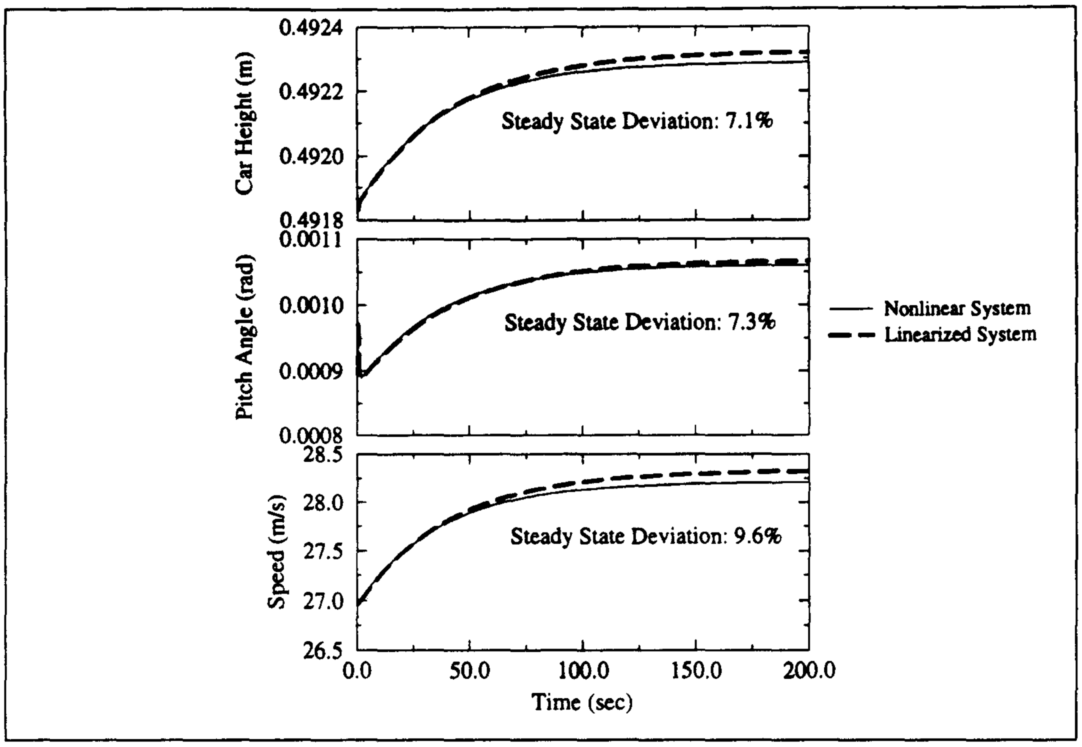

Figure 8.23: Effect of perturbation size on numerical derivative computation.

Figure 8.25 shows the vehicle roll angle, yaw velocity and path. As the vehicle turns left, the vehicle should roll to the right, for a positive roll angle, and the yaw velocity should increase to reach a constant in steady state as seen in Figure 8.25. At this speed, a turn of 0.01 radian is considered to be a medium cornering maneuver which generates a lateral acceleration of about 0.2g. If the vehicle is allowed to reach steady state, a constant steering angle of 0.01 radian will steer the vehicle around a constant radius of 310 meters.

Next, lateral response is examined as a pulse of crosswind is applied to the vehicle while the vehicle is traveling straight ahead at $27\frac{m}{sec}$. The applied wind velocity is $15\frac{m}{sec}$ with 10 seconds duration. The lateral response of the vehicle is plotted in Figure 8.26, showing the vehicle path without any steering correction is made. Plots of the crosswind profile and yaw velocity are also shown. The decrease in the yaw velocity reflects that the magnitude of the side wind applied to the vehicle is decreasing since the vehicle is gradually turning away from the crosswind disturbance.

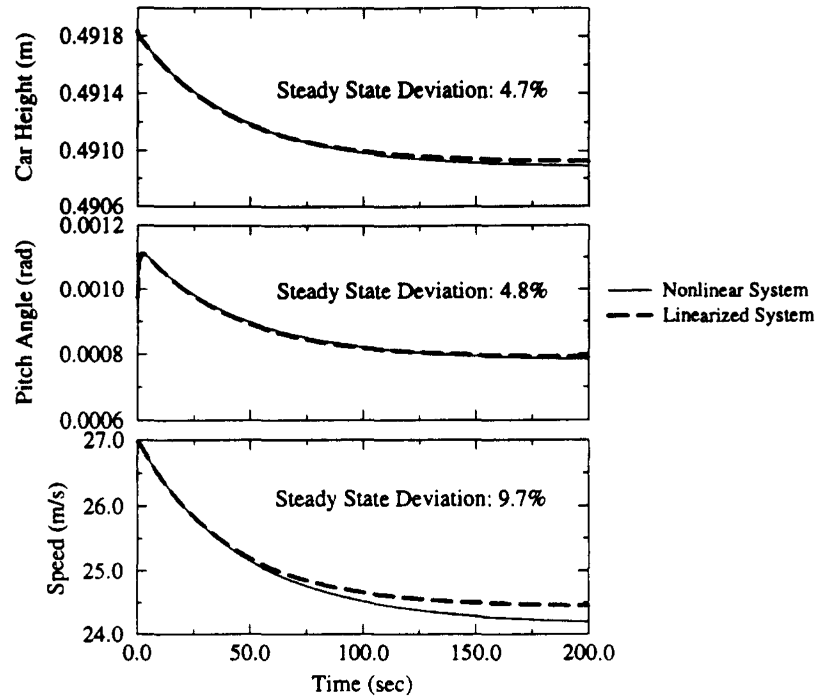

Figure 8.24: Steady-state response of the linearized and nonlinear systems with a perturbed brake input (+34 N).

Finally, random road excitation is introduced to the vehicle model, simulating the road condition of typical highways. The vehicle roll and pitch angle as well as its height are shown in Figure 8.27 together with the random road excitation of the right and left tracks. The left and right tracks are taken to have the same spectral density function and are also correlated, with the correlation coefficient having a value of 0.75. Averaging from 100 realizations, the simulated spectral density of the random processes are plotted along with the theoretical density in Figure 8.28. Similarly, the coherency functions which characterize the dependency between the left and right tracks are also shown on lower half of Figure 8.28. Looking at the road noise of the left and right tracks, one can see that they are highly correlated at low frequencies. On the other hand, high frequency components of the noise do not seem to be correlated between left and right tracks. An alternative way to look at this is by the means of the coherency function as seen in Figure 8.28. At low wave number or spatial frequency, the left and right tracks are strongly correlated and the coherency function rapidly decreases as the wave number increases.

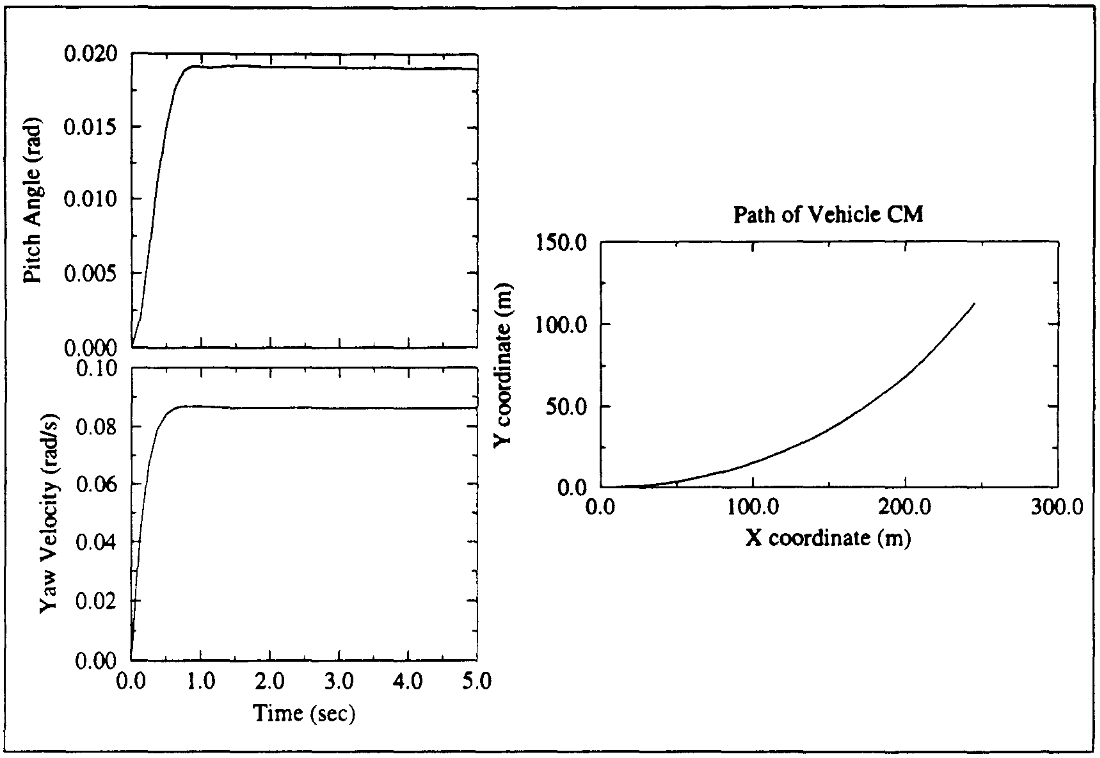

Figure 8.25: Vehicle response due to step steering input of 0.01 radian.

Small Angle Approximation

We would like to investigate the effects, if any, of a small angle approximation of the pitch and roll angles, on the accuracy of the full model simulation. We have already established that the operating range of the pitch angle is small enough that a small pitch angle approximation does not have a significant effect on the simulation accuracy of the vehicle model. The operating range of the roll angle is similar to that of the pitch angle. Therefore we should also expect that making a small angle approximation to the roll angle does not significantly reduce the model accuracy. Again we would like to find out under what situations the vehicle might experience a large roll angle. During high lateral acceleration, the maximum limit of the roll angle relative the ground surface can be at most around

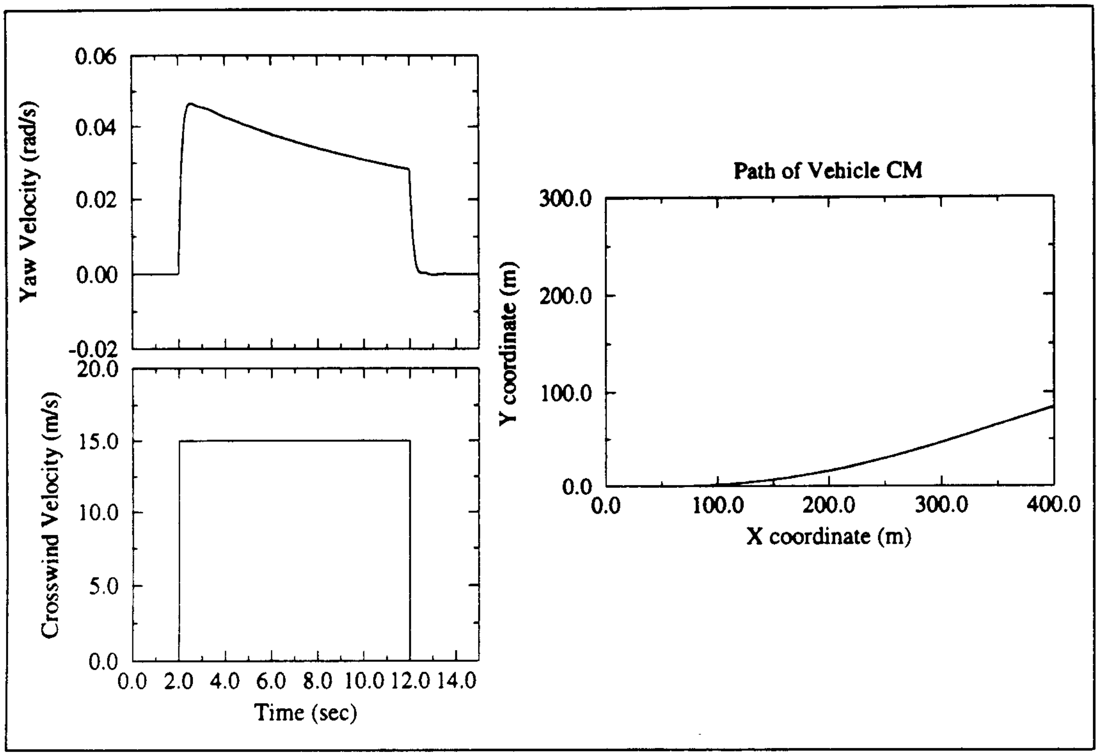

Figure 8.26: Vehicle response due to a crosswind pulse of $15\frac{\text{m}}{\text{sec}}$.

0.05 radians. Since roll angle in the model is the sum of the relative roll and the road superelevation, it is also necessary to obtain the maximum limit of the road superelevation. Usually on regular highways, road superelevations are quite small, typically under 1%. The only sections of the highway system where the road superelevation may be large are the ramps connecting one highway to another. Nevertheless the superelevation of these ramps are not large either. They are at most on the order of a few percent. To be on the conservative end, we will use a road superelevation of 10% in our simulation to test the effect of making a small angle approximation of the roll angle.

The roll angle of the vehicle is plotted in Figure 8.29 as the vehicle is traveling on a planar road with a superelevation of 10% and the vehicle is initially rolled to the right by 0.05 radians relative to the road surface. This sets the initial condition of the roll angle to approximately 0.15 radians. As shown in Figure 8.29, there is no noticeable deviation of the response between the approximated and the non-approximated system. The maximum difference of the pitch angle between the two models is below two orders of magnitude. In addition, the maximum error during transient response for any states is 2%, and during steady state is much lower. Therefore, we conclude that it is reasonable to make a small angle approximation of the roll angle.

Since the yaw angle can have any value, it is incorrect to use a small angle approximation of the yaw angle. By making small angle approximation to the pitch and the roll angle, we can achieve a 1% reduction in computation time. The reason that this improvement is less than that in the longitudinal model is because the sub-components are more complicated and there are more of them. In summary, it is reasonable to use a small angle approximation of the pitch and roll angles. While the savings in computational time is minimal it is welcome.

Linearization Around a Constant Steering Angle

At some point during a trip, the vehicle will have to travel along a curve, which can be a curvy stretch of freeway or a transition ramp from one freeway to another. Therefore it is necessary to have a linearized model for fault detection and identification system to process as the vehicle is traveling through a curved path. Each path can be considered as a constant radius curve, hence we can linearize our model around a constant steering angle.

The linearization process is identical to that of the longitudinal case except that one must be more careful in choosing the perturbation size for each coefficient. The acceptable range for perturbation size now becomes smaller and is different for each coefficient. As shown previously, it is best to plot each coefficient versus the perturbation size and pick the coefficient at the appropriate region.

Once the linearized model is obtained at some nominal operating point, we can proceed to measure the effective range of the linearized model which can reproduce the response of the nonlinear model within a 10% error in all of the states. First, a linearized model is obtained from the nonlinear model when the vehicle is traveling straight ahead. No further investigation of the longitudinal response is required since it was already done in

Section 8.3.1. Figure 8.30 shows the longitudinal speed, lateral speed and yaw angle of the vehicle when the steering angle is perturbed by 0.01 radians. Even for a relatively large perturbation of the steering angle, the yaw rate of the linearized model matches very well that of the nonlinear model.

On the other hand, the steering input has no effect on the longitudinal velocity in the linearized model. The reason is that a linear system is incapable of modeling even symmetric responses of a nonlinear system. An even symmetric response is characterized by an output that is affected only by the magnitude and not by the direction of the input. Therefore all the modes that exhibit even symmetric behavior around zero steering angle input will be not be captured by the linearized model. The longitudinal velocity is such a mode, hence it is unaffected by any amount of perturbation applied to the steering angle. The modes that are not even symmetric are the lateral and yaw velocities. Thus a perturbation in the steering angle will directly perturb these modes as shown in Figure 8.30. Also apparent in the plot is that the yaw velocity response is much more linear than the lateral velocity in response to a steering input. With this in mind, a system linearized around a zero steering angle must be used with caution in situations where a perturbation in steering angle might be present.

Next, the system is linearized around a constant steering angle of 0.005 radians which will steer the vehicle around a constant radius curve of 620 meters at steady state. This results in a gentle lateral acceleration of about 0.1g while the vehicle is traveling at a constant speed around $26.5\frac{\text{m}}{\text{sec}}$. To achieve a maximum limit of 10% error between the nonlinear and the linearized system in all the significant states at steady state, the range of the perturbation size for each input variable is found and tabulated in Table 8.2. In addition, some responses of the perturbed system between the linearized and the nonlinear systems are compared. Figure 8.31 shows the responses of the longitudinal, lateral, and yaw velocities as the throttle position is increased by 15 percent. The most nonlinear state is the yaw velocity, since it is not directly affected by the throttle position but, rather, indirectly coupled with other states which can be directly or indirectly driven by the throttle position. In addition, a perturbation in the brake should also produce similar results as seen in Figure 8.32. As discussed in Section 8.3.1, the responses of the nonlinear system due to brake input are more linear than those due to throttle input. Hence, one should expect that the response of the linearized model due to a brake perturbation covers a wider range such that the steady state errors between the linearized and nonlinear system can be at most 10% when a step input is applied. Lastly, the vehicle longitudinal, lateral, and yaw velocities are plotted in Figure 8.33. Now the yaw velocity is directly coupled with the steering angle. Therefore one can expect that the response of the yaw angle is quite linear with respect to a perturbation of the steering angle. This can be clearly observed in Figure 8.33.

0 rad.	-15% to +15%	N/A	0 to 34N
0.005 rad.	-14% to +14%	-15% to +25%	0 to 27N

Table 8.2: Effective range of the linearized system.

Unlike the system linearized around a zero steering angle, this system is able to capture part of the coupled dynamics between the longitudinal and lateral motion. The reason is that the even symmetric modes around a zero steering angle are not symmetric around 0.005 steering angle. Therefore the linearized system can model the nonlinear system more accurately when the odd symmetric modes are dominant.

8.4 Summary of Model Development and Suggestions for Future Work

Two vehicle dynamics models have been developed using analytical mechanics. One is a simplified longitudinal model and the other is a full lateral and longitudinal model. The vehicle models include all major components including the suspension, tire traction, engine, brake and steering models. In addition, the model allows for arbitrary road gradient variations. Random road excitation is introduced using a first-order shaping filter approach.

In looking for ways to reduce computational complexity, a simulation study showed that small angle approximations do not significantly affect the accuracy of the simulation.

However, the same simulation study indicated no substantial reduction in computational time is realized by this approximation. Lastly, linearized vehicle dynamic models at various operating points, including straight and curved paths, are derived numerically.

The following suggestions are recommended for future work in order to refine and incorporate more features in the vehicle model. First, only a theoretical model is developed here and unfortunately vehicle parameters from different sources are used. Hence it is important to experimentally obtain all the vehicle parameters from a single test vehicle and then validate the theoretical model using experimental data. In any development process it is impossible to include all of the vehicle features at once. The list below covers the important items which have been omitted and therefore require further investigation.

- Change in steering angle due to suspension geometry.
- Linear stabilizers.
- Modeling of the unsprung mass.
- Modeling of the wheel mass.
- Static camber.
- Dynamic camber induced by suspension movement.
- Static toe-in.
- Dynamic toe-in induced by suspension movement.

Since this vehicle model will be used in fault detection filter design and evaluation, it is important to be able to model malfunctions or total failures in critical vehicle components. Modeled failures might include, for example, a flat tire, brake failure, engine malfunction and out-of-alignment steering. This development is especially important to health monitoring system evaluation applications.

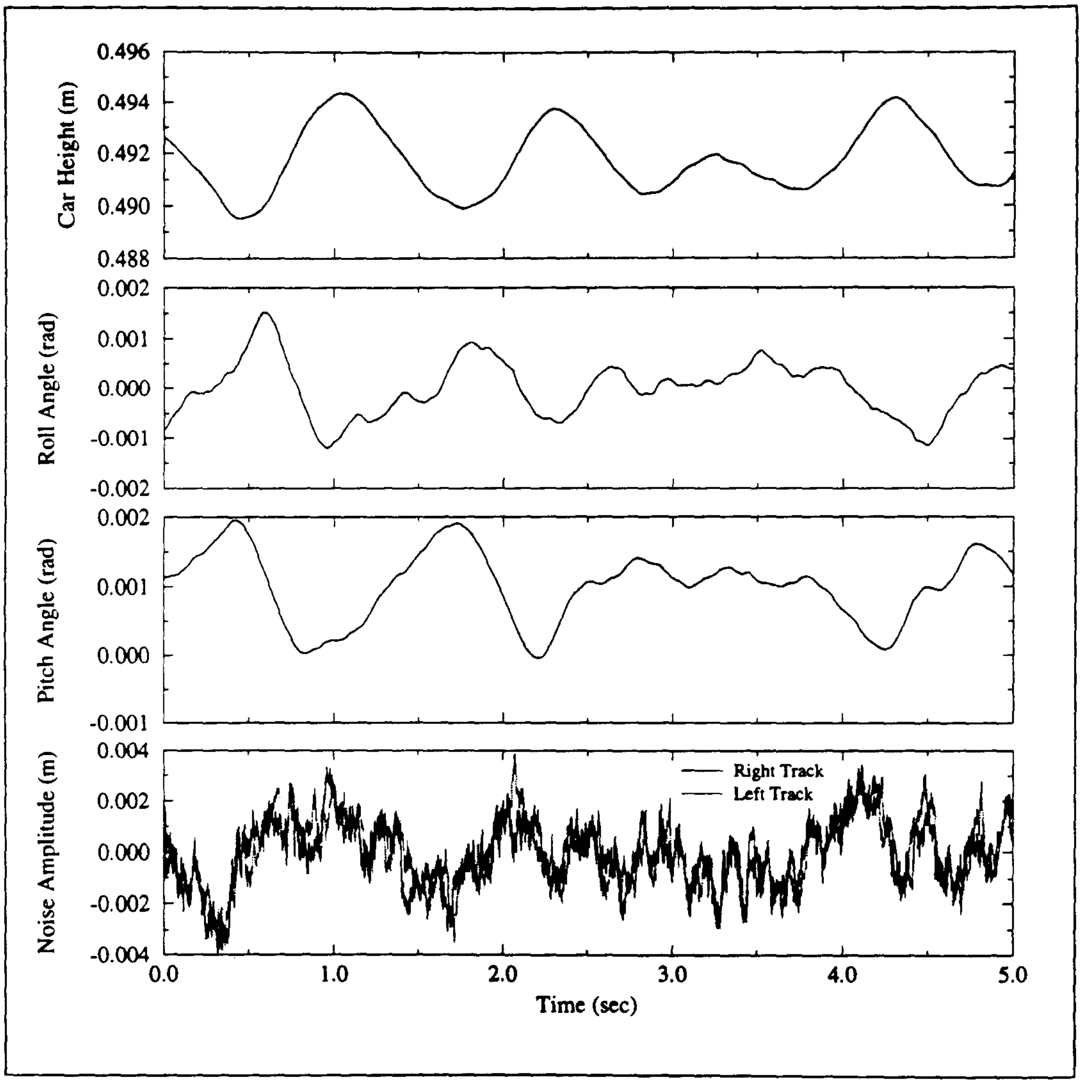

Figure 8.27: Vehicle response due to road noise.

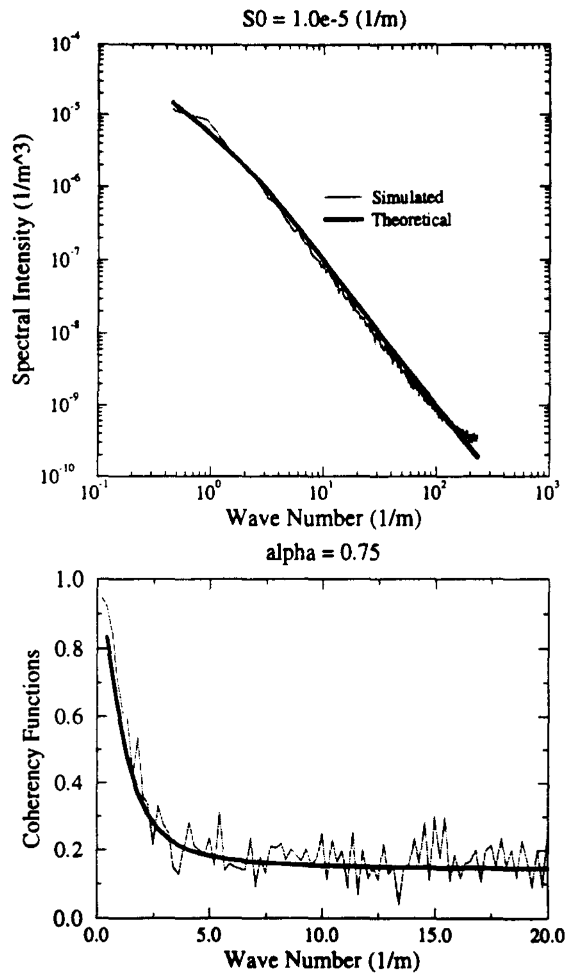

Figure 8.28: Spectral densities and coherency functions of left and right tracks.

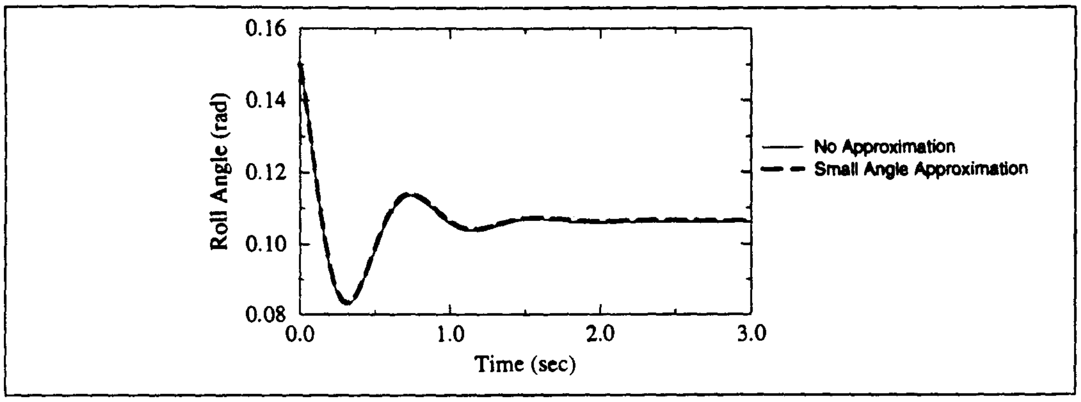

Figure 8.29: Effect of making a small angle approximation of the roll angle.

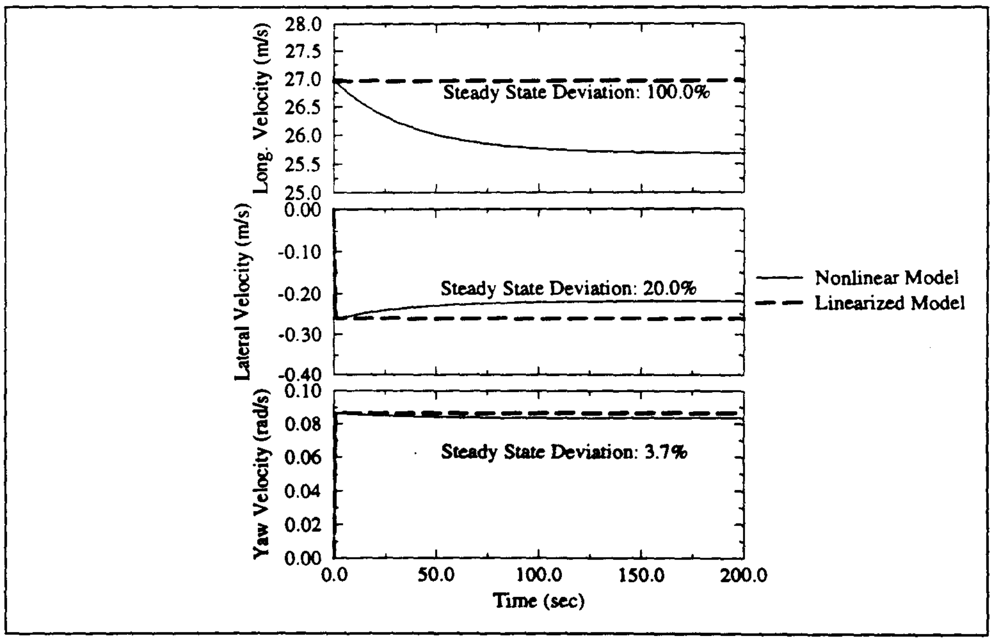

Figure 8.30: Comparison of vehicle linearized and nonlinear system responses where steering angle is perturbed by 0.01 radian.

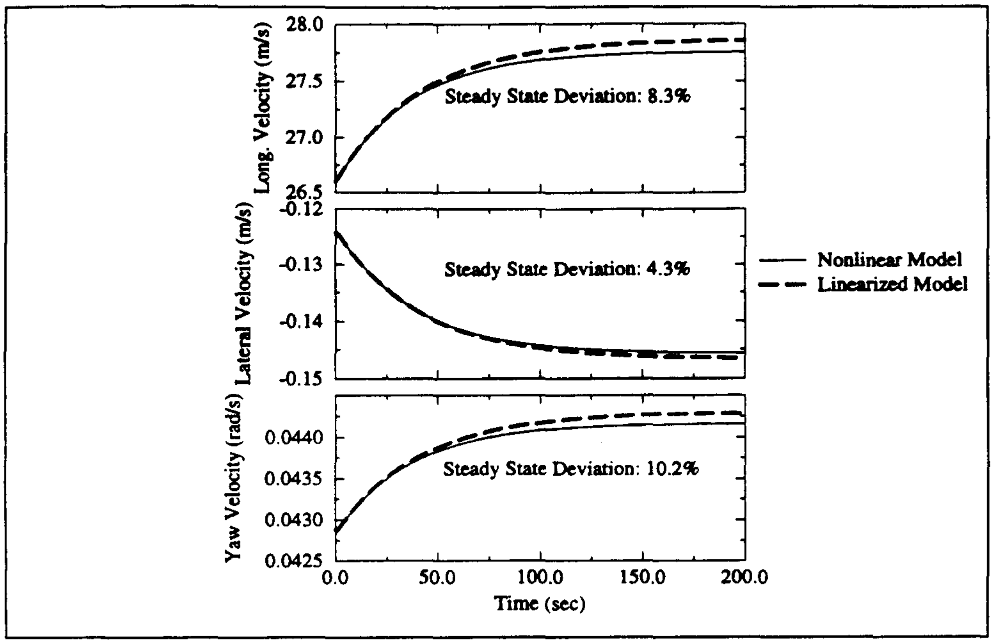

Figure 8.31: Comparison of vehicle linearized and nonlinear system responses where throttle position is perturbed by 15%.

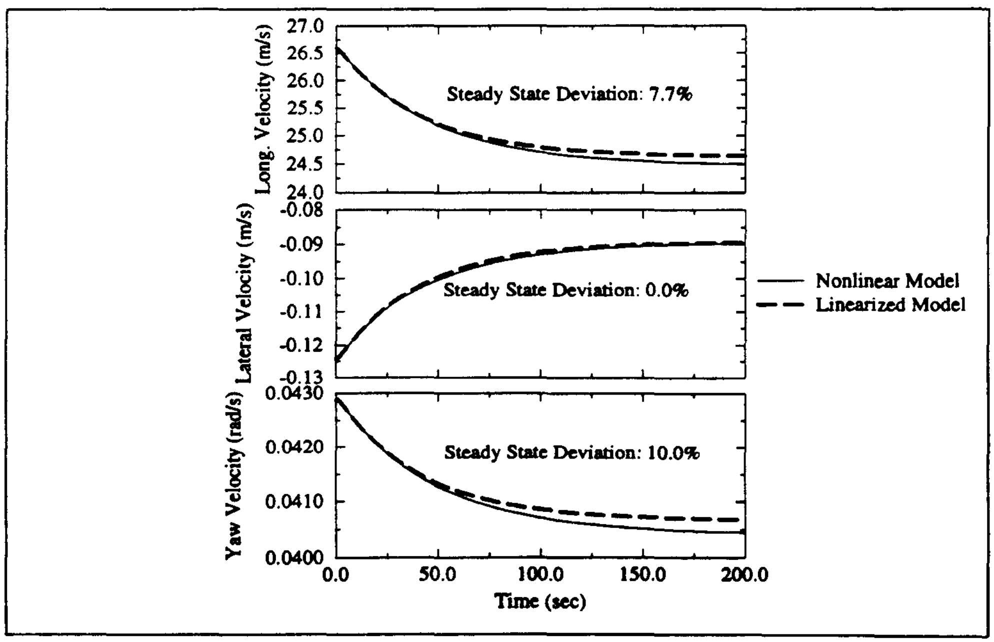

Figure 8.32: Comparison of vehicle linearized and nonlinear system responses where brake torque is perturbed by 27 N.

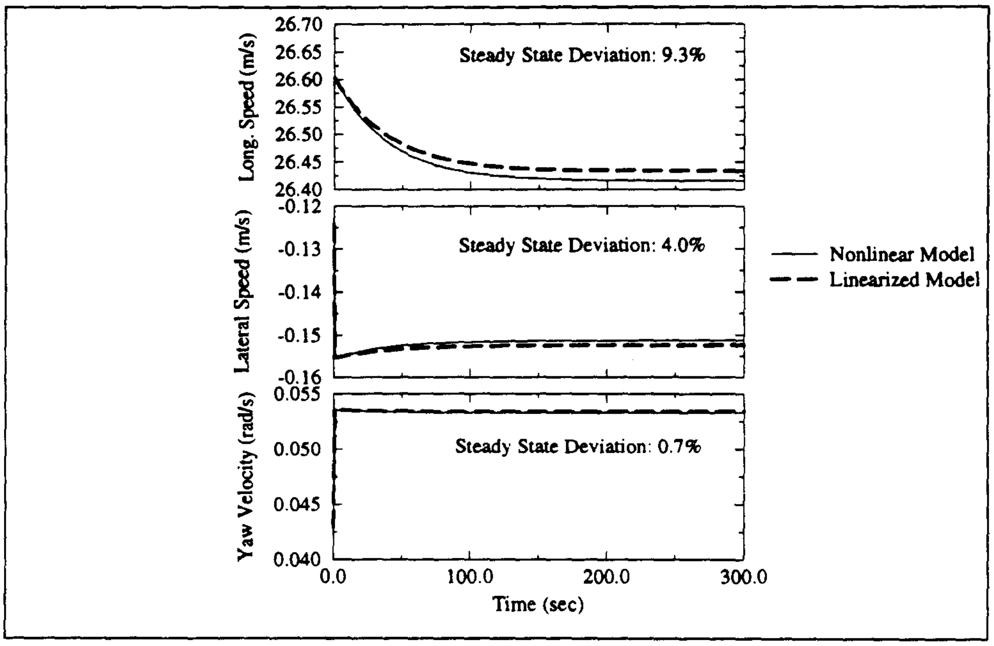

Figure 8.33: Comparison of vehicle linearized and nonlinear system responses where steering angle is perturbed by 25%.